Impact of Fuel Rod Coatings on Reactor Performance and Safety

A Thesis Presented for the

Master of Science

Degree

The University of Tennessee, Knoxville

Ian Robert Stewart

May 2015

Acknowledgements

Foremost, I would like to thank my advisor and committee chair, Dr. Laurence F. Miller, for his support throughout this process. His patience and encouragement in the beginning proved to be vital in giving me a direction for my research.

I would also like to thank Dr. Ronald Pevey and Dr. Brian Wirth for being on my committee and giving me honest feedback when and where it was required. Their time and opinions were crucial to the completion of this thesis and my Master's degree.

A sincere thanks for Dr. Kurt Sickafus for trusting me to present on my material on behalf of the NEUP project. Furthermore, none of this would be possible without the financial support from the Nuclear Energy University Program - Integrated Research Projects (NEUP-IRP).

Lastly, I want to thank my family and friends for helping shape me into who I am today.

Abstract

This study evaluates the use of a ceramic coating on the Zr-alloy cladding within a PWR using four ceramic compounds of 5 and 10 micron thicknesses: ZrO2, TiAlN, Ti2AlC, and Ti3AlC2. The film's impact is assessed for variation on: reactivity, fuel cycle length, maximum temperature, film's roughness, and transient conditions. The reactivity is analyzed using the following methods: change in the multiplication factor (k) each film introduces to the system using the ABH method, and Monte Carlo software (MCNP). Both methods are in good agreement, yielding less than half a percent change from a reference, no-film fuel pin. In order from lowest impact to highest impact on reactivity, the films are as follows for 10 micron thickness: ZrO2 (0.06%), TiAlN (0.20%), Ti3AlC2 (0.21%), and Ti2AlC (0.25%). This change directly impacts the fuel cycle length of the fuel. A linear reactivity model is used to approximate the loss in fuel cycle length and final burnup for a reference cycle of 300 days and 50 MWd/kg, respectively. The estimated loss in days is less than a day for all 5-micron films and less than 3 days for all 10 micron films (*highest*: 2.25 days, Ti2AlC) with all burnup calculations around 48.50 MWd/kg for all films. The impact the film yields on the temperature of the fuel pin is calculated using the one-dimensional thermal resistance circuit for each region (fuel, gap, clad, film, and moderator). The films' thermal conductivity will directly impact this calculation, yet for the thin ceramic films, the percent change from a reference fuel is less 1% for all films at both thicknesses (largest change, lowest thermal conductivity: ZrO2). The roughness of the films currently being deposited is around 10 microinch Ra. This value is used with two perturbations, 5 microinches and 15 microinches**,** to evaluate the impact on the heat transfer coefficient and the induced friction-loss (pressure). For all roughness values the heat transfer coefficient stays well within typical PWR values while inducing a smaller pressure drop along the channel (compared to Zr-alloy clad). The thermal analysis is used to simulate a transient by varying the linear power density and the coolant flow rate. These two parameters are varied at different rates to impose a momentary mismatch in the system. In all simulations, the film reacts almost identical of that of the Zr-alloy clad reference model.

Table of Contents

1: Introduction 1
2: Methodology 3
2.1: Reactivity / Multiplication Factor 3
2.2: Fuel Cycle Length 9
2.3: One-Dimensional Fuel Temperature 11
2.4: Film Roughness 16
2.5: Uncertainty Analysis 19
2.6: Fuel and Coolant Temperature during Transients 23
3: Results 26
3.1: Reactivity Impact 26
3.2: Loss in Fuel Cycle Length 30
3.3: Fuel Maximum Temperature 31
3.4: Film Roughness Impact 33
3.5: Parameter Uncertainty Analysis 35
3.6: Temperature Change during Flow Transient 37
4: Conclusion 46
5: Future Work 47
Works Cited 48
Appendix 50
Vita 64

List of Tables

Table 1: Triangular Distribution Parameters for an example uncertainty values for ZrO_2 film. .. 21
Table 2: Geometric parameters of reference fuel pin and coating. 27
Table 3: Film properties. 28
Table 4: Absorption cross section for proposed ceramic films. 28
Table 5: Analysis of 5 micron and 10 micron thick film region with the ABH method..... 29
Table 6: Reactivity impact from 5 and 10 micron thick film. 30
Table 7: Estimated loss fuel cycle length based on a 900 day cycle and fuel burnup. 31
Table 8: Parameters for the calculation of temperature changes in a fuel pin. 32
Table 9: Thermal conductivity of proposed coatings 32
Table 10: Impact on fuel centerline temperature for each film at 5 and 10-micron thickness..... 33
Table 11: Physical properties of water coolant 34
Table 12: Impact on heat transfer coefficient with various film friction factors. 34
Table 13: Pressure drop induced by film roughness along the flow channel. 35
Table 14: Uncertainty obtained for ABH method and centerline temperature. 36
Table 15: Multiplication factor and centerline temperature with uncertainty. 37
Table 16: Depletion of each film isotope using constant power approximation equation. 53
Table 17: Isotropic Depletion using constant flux approximation equation. 54
Table 18: Multiplication factor with varying boron concentration ratios at 10-micron film. 55
Table 19: Multiplication factor for different boron concentration ratios at 100-micron film. 55
Table 20: Reactor Information from Duderstadt text Appendix H 56

List of Figures

Figure 1: Five categories that require consideration for new fuel designs..... 2
Figure 2: Fuel geometry used in obtaining PMF. 7
Figure 3: Parameters used in ABH method..... 8
Figure 4: Linear Relationship of reactivity and burnup at a nominal initial reactivity. 9
Figure 5: Reactivity vs. Burnup relationship obtained from the EPRI 10
Figure 6: Electrical circuit analogy for thermal resistance across a cylindrical fuel pin 11
Figure 7: Moody diagram illustrating relationship between friction factor, relative surface roughness, and flow parameters. 17
Figure 8: Flow of a Monte Carlo simulation for ABH method to calculate the thermal utilization factor..... 22
Figure 9: Monte Carlo simulation for fuel temperature calculation for the heat transfer coefficient and thermal conductivity of the film. 22
Figure 10: No-film region simulation illustrating the two varying parameters and the impact on the moderator temperature change along the channel. 38
Figure 11: Power transient followed by slower velocity change using 10μm ZrO2 film. 40
Figure 12: Power transient followed by slower velocity change using 10μm TiAlN film. 40
Figure 13: Power transient followed by slower velocity change using 10μm Ti2AlC film. 41
Figure 14: Power transient followed by slower velocity change using 10μm Ti3AlC2 film. 41
Figure 15: Reference run for flow velocity variation followed by power density. 42
Figure 16: Flow velocity transient followed by slower power density change using 10μm ZrO2 film and lower heat transfer coefficient. 43
Figure 17: Flow velocity transient followed by slower power density change using 10μm TiAlN film and lower heat transfer coefficient. 43
Figure 18: Flow velocity transient followed by slower power density change using 10μm Ti2AlC film and lower heat transfer coefficient. 44
Figure 19: Flow velocity transient followed by slower power density change using 10μm Ti3AlC2 film and lower heat transfer coefficient. 44
Figure 20: Depletion of a single isotope comparison using constant flux and constant power approximations. 51

1: Introduction

The current fleet of light water reactors (LWRs) in the United States uses a UO_2 fuel and a Zr-alloy, or Zircaloy, cladding material. The fuel element design and reliability is a key aspect to maintaining a safe, cost-competitive source of power. In order keep nuclear energy as a key component for power production in the future, continuous research and development is vital. The *Nuclear Energy Research and Development Roadmap* prepared by the United States Department of Energy (DOE) organizes the future challenges of the nuclear industry into four categories: [1]

> " 1. *develop technologies and other solutions that can improve the reliability, sustain the safety, and extend the life of current reactors;*
> 2. *develop improvements in the affordability of new reactors to enable nuclear energy to help meet the Administration's energy security and climate change goals;*
> 3. *develop sustainable nuclear fuel cycles; and*
> 4. *understanding and minimization of risks of nuclear proliferation and terrorism*. "

With the recent nuclear accident suffered at the Fukushima Dai-ichi nuclear facility in March of 2011, renewed interest in fuel design has been brought to the forefront once again. During the events that occurred at the Fukushima Dai-ichi facility, the Zr-alloy cladding underwent severe oxidation reactions due to the high temperature water around the fuel, creating large amounts of hydrogen. [1,2] From the lessons learned from the Fukushima Dai-ichi accident, alternative fuel and cladding concepts are being developed in order to enhance the safety of the reactor, competiveness, and economics of the current power reactor fleet. These new fuel/clad concepts is a part of the Accident Fuel Campaign and have been given the name Accident Tolerant Fuels (ATF) by the nuclear industry. The purpose of the ATFs is to increase the safety of the reactor system during beyond-design-basis accidents (e.g. loss of coolant accidents) and increase the time before fuel failure, all while improving, or remaining reasonably close to the conventional

UO_2-Zr, the system during normal operations (e.g. economics, reliability, spent fuel management). To accomplish these tasks, various concepts have been proposed, such as: silicon-carbide clad, various iron-based alloys for clad, refractory materials, additional film region applied to Zr-clad, and numerous UO_2 fuel replacements. [2,3]

This study evaluates an applied thin ceramic film to the moderator side of the Zr-clad within a PWR. This concept proposes an ATF notion that can be implemented in the currently operating reactors, with minimal design change required. This backward-compatibility is essential to implementing a new fuel design. The figure below illustrates the issues that must be addressed in order to employ a new fuel concept. [2,4]

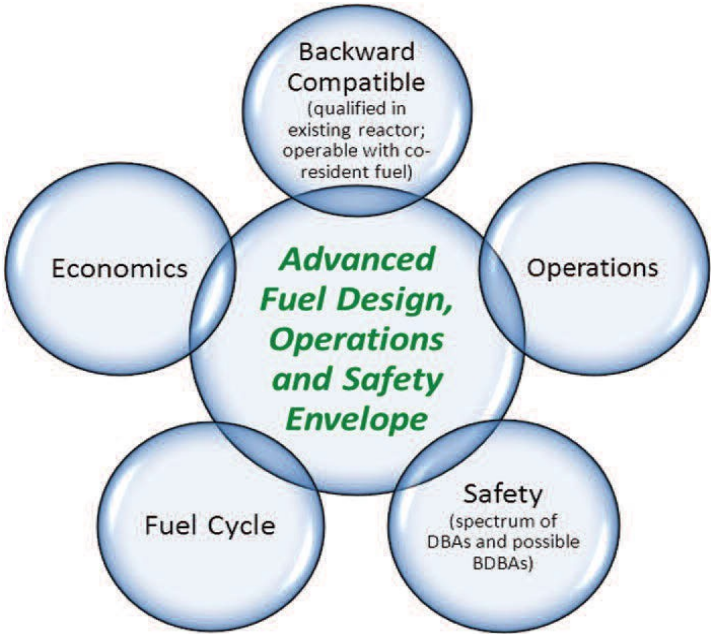


Figure 1: Five categories that require consideration for new fuel designs. [1]

This report addresses some of these considerations for various ceramic films at various thicknesses.

2: Methodology

This study examines four ceramic films at thicknesses of 5 and 10 micron. The proposed films include:

1. ZrO_2,
2. TiAlN,
3. Ti_2AlC, and
4. Ti_3AlC_2.

The addition of a film region will introduce changes to the neutronic and thermal characteristics, of the fuel. In particular, impacts of these films on the following neutronic and thermal hydraulic operational and safety parameters are reported:

1. Reactivity,
2. Fuel Cycle Length,
3. Fuel Centerline Temperature,
4. Film roughness, and
5. Impact on Fuel and Coolant Temperature during Transients.

Uncertainty analysis is implemented via Monte Carlo sampling techniques of uncertain parameters to illustrate the confidence of the calculations.

2.1: Reactivity / Multiplication Factor

The addition of a ceramic film region to the moderator-side of the cladding will impact the neutron economy in the reactor. In terms of expressing the neutronic impact, this project evaluates the multiplication factor (k) which gives the ratio of number neutrons in one generation to the number of neutrons in the preceding generation. Moreover, we calculate the multiplication

factor (k), assuming infinite medium (k_∞), which can be expressed in a *four-factor formula* given in Equation 1 (neglecting leakage terms):[5]

$$k_\infty = \eta f p \epsilon \qquad \text{(Eq.1)}$$

where, η is the reproduction factor, f is the thermal utilization factor, p is the resonance escape probability, and ϵ is the fast fission factor. It is beneficial at this point to expand each term in the equation in order to understand the effect the ceramic film will induce on each: [5,6]

Reproduction factor (η): number of fission neutrons produced per absorption in the fuel, $\eta = \nu\ (\ \sigma_{\mathrm{f}}^{\mathrm{F}}/\sigma_{\mathrm{a}}^{\mathrm{F}}\ )$

Thermal utilization factor (f): ratio of the macroscopic cross sections of the fuel to the macroscopic of the fuel plus the remaining material in the core (i.e. probability that a thermal neutron is absorbed by the fuel), $f = \Sigma_a^F/\Sigma_a$

Resonance escape probability (p): fraction of fission neutrons that manage to slow down from fission to thermal energies without being absorbed

Fast fission factor (ϵ): ratio of the total number of fission neutrons (from both fast and thermal fission) to the number of fission neutrons from thermal fissions.

The ceramic film will have minor effects on the reproduction factor, resonance escape probability, and the fast fission factor. Therefore, further consideration in the thermal utilization factor is evaluated and, if we assume there is no change in the other three parameters in the four-factor formula, the thermal utilization will represent the impact the film has on the system. Directly, the thermal utilization change will yield the impact the film introduces on the neutron economy, and it can be expanded to illustrate how each region will present an impact:

$$f = \frac{\phi_{fuel}\Sigma_{\mathrm{abs}}^{fuel}V_{fuel}}{\phi_{fuel}\Sigma_{fuel}V_{fuel}+\phi_{mod}\Sigma_{\mathrm{abs}}^{mod}V_{mod}+(\phi\Sigma V)_{rest}}\ , \qquad \text{(Eq.2)}$$

where, ϕ represents the neutron flux in the respective region, Σ_{abs} is the absorption cross section, and V is the volume fraction. The other regions (e.g. gap, clad, film) can be lumped into the $(\phi\Sigma V)_{rest}$ variable. However this method expressed in Equation 2 results in poor estimates changes of the thermal utilization due to adding a coating. [5,6] An alternative analytical scheme based on transport theory proposed by Amouyal, Benoist, and Horowitz, referred to as the ABH method, is used to expand the thermal utilization factor. The ABH method uses an approximation of the probability that a neutron escaping the fuel will be absorbed in the moderator (β_{M}) expressed in Equation 3: [5]

$$\beta_{\text{M}} = \left(\frac{\text{V}_{\text{M}}}{\text{V}_{\text{F}}}\right)\left(\frac{\Sigma^{\text{M}}_{abs}}{\Sigma^{\text{F}}_{abs}}\right)\left(\frac{P_{\text{MF}}}{P_{\text{F}}}\right) \quad \text{(Eq.3)}$$

where, Σ^{F}_{abs} and Σ^{M}_{abs} represent the absorption macroscopic cross section for the fuel and moderator region respectively, $\frac{V_{\text{M}}}{V_{\text{F}}}$ represents the moderator to fuel volume fraction, P_{MF} is the transfer probability characterizing source neutrons born in the moderator and absorbed in the fuel, and $P_{\text{F}}$is the probability that a neutron born in the fuel escapes the fuel before being absorbed.

In order to obtain β_{M}, the terms P_{MF} and P_{F} are required. Assuming a large (compared to mean free path), purely absorbing fuel lump, the P_{F} can be approximated as [5]

$$P_{\text{F}} \cong \frac{S_{\text{F}}}{4V_{\text{F}}\Sigma^{\text{F}}_{abs}} \quad \text{(Eq.4)}$$

where S_{F} represents the surface area of the fuel region. Thus, β_{M} can now be rewritten as

$$\beta_{\text{M}} = \frac{4\Sigma^{\text{M}}_{abs}V_{\text{M}}}{S_{\text{F}}}P_{\text{MF}}. \quad \text{(Eq.5)}$$

From Duderstadt text: Assuming that "all thermal neutrons first appear as a slowing down source uniformly distributed in the moderator, the thermal utilization is then just the probability characterizing source neutrons born in the moderator and absorbed in the fuel", or P_{MF}. [5]

$$f = P_{\mathrm{MF}} = \left(\frac{V_{\mathrm{F}}}{V_{\mathrm{M}}}\right)\left(\frac{\Sigma_{abs}^{\mathrm{F}}}{\Sigma_{abs}^{\mathrm{M}}}\right) P_{\mathrm{FM}} \tag{Eq.6}$$

Where, P_{FM} describes the probability that a neutron born in the fuel will eventually be absorbed in the moderator region. [5] This probability is expressed as the product of the β_{M} and P_{F}, the probability that a neutron in the fuel will be eventually absorbed in the fuel.

$$P_{\mathrm{FM}} = P_{\mathrm{F}}\, \beta_{\mathrm{M}} \tag{Eq.7}$$

Combining Equations 5 and 6, we obtain a new equation for the thermal utilization factor. [5]

$$f = \left(\frac{V_{\mathrm{F}}}{V_{\mathrm{M}}}\right)\left(\frac{\Sigma_{abs}^{\mathrm{F}}}{\Sigma_{abs}^{\mathrm{M}}}\right) P_{\mathrm{F}}\, \beta_{\mathrm{M}} \tag{Eq.8}$$

Equation 7 can then be rewritten using Equation 4 and 5:

$$\left(\frac{1}{f} - 1\right) = \left(\frac{\Sigma_{abs}^{\mathrm{M}}}{\Sigma_{abs}^{\mathrm{F}}}\right)\left(\frac{V_{\mathrm{M}}}{V_{\mathrm{F}}}\right)\frac{1}{P_{\mathrm{F}}} + \frac{1 - P_{\mathrm{MF}}}{P_{\mathrm{MF}}} - \frac{4\Sigma_{abs}^{\mathrm{M}} V_{\mathrm{M}}}{S_{\mathrm{F}}} \tag{Eq.9}$$

The key idea involved in the ABH method is obtaining a crude scheme to obtain P_{MF}. This is accomplished by using diffusion theory with transport-corrected boundaries between the fuel-moderator regions. [5] This is achieved by solving Equation 10

$$D_{\mathrm{M}} \nabla^2 \phi_{\mathrm{M}}(\boldsymbol{r}) - \Sigma_{abs}^{\mathrm{M}} \phi_{\mathrm{M}}(\boldsymbol{r}) = -q_0 \tag{Eq.10}$$

and using the boundary conditions:

$$\left.\frac{d\phi_{\mathrm{M}}}{dr}\right|_{r=b} = 0 \quad , \tag{Eq.11}$$

$$\left.\frac{1}{\phi_{\mathrm{M}}}\frac{d\phi_{\mathrm{M}}}{dr}\right|_{r=a} = \frac{1}{d} \quad , \tag{Eq.12}$$

where D_{M} is the diffusion coefficient in the moderator region, ϕ_{M} is the flux within the moderator, q_0 is the linear power density, d is a transport boundary correction, and a/b are radial values from Figure 2. [5,6]

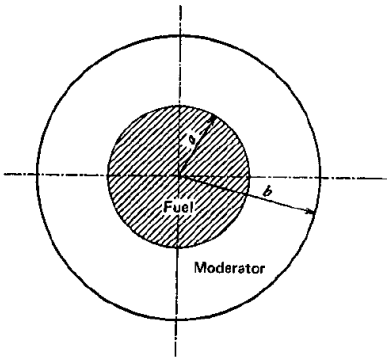


Figure 2: Fuel geometry used in obtaining P_{MF}.

Assuming $P_{\mathrm{MF}} \sim P_{\mathrm{M}}$, we need to solve for P_{M}.

$$P_{\mathrm{M}} = \frac{2\pi a D_{\mathrm{M}}}{q_0 V_{\mathrm{M}}}\left.\frac{d\phi_{\mathrm{M}}}{dr}\right|_a \tag{Eq.13}$$

Sparing the details of solving the diffusion equation and the P_{M} probability, the final result is given by

$$P_{\mathrm{M}} = \left\{\frac{V_{\mathrm{M}} a d}{2V_{\mathrm{F}} L_{\mathrm{M}}^2} + \mathrm{E}\left(\frac{a}{L_{\mathrm{M}}}, \frac{b}{L_{\mathrm{M}}}\right)\right\}^{-1} \cong P_{\mathrm{MF}} \tag{Eq.14}$$

where $L_M^2 = D_{\mathrm{M}}/\Sigma_{abs}^{\mathrm{M}}$ and $\mathrm{E}(\ldots)$ is the lattice function, which in this case will be in cylindrical form. [5] Combining the equations, we arrive at the final expression of the ABH method:

$$\frac{1}{f} = \frac{\Sigma_{abs}^{\mathrm{M}} V_{\mathrm{M}}}{\Sigma_{abs}^{\mathrm{F}} V_{\mathrm{F}}}\left\{1 + \frac{\Sigma_{abs}^{\mathrm{F}}}{\Sigma_{tot}^{\mathrm{F}}}\left[\frac{1-P_{\mathrm{FO}}}{P_{\mathrm{FO}}} - a\Sigma_{tot}^{\mathrm{F}}\right]\left[1 + a\left(\frac{\Sigma_s^{\mathrm{F}}}{\Sigma_{tot}^{\mathrm{F}}}\right) + \beta\left(\frac{\Sigma_s^{\mathrm{F}}}{\Sigma_{tot}^{\mathrm{F}}}\right)^2\right]\right\} + \left(\frac{ad}{2L_{\mathrm{M}}^2} - a\Sigma_a^M\right)\left(\frac{V_{\mathrm{M}}}{V_{\mathrm{F}}}\right) + E\left(\frac{a}{L_{\mathrm{M}}}, \frac{b}{L_{\mathrm{M}}}\right) \quad , \qquad \text{(Eq.15)}$$

where α and β are parameters for cylindrical geometries given in Figure 3. [5]

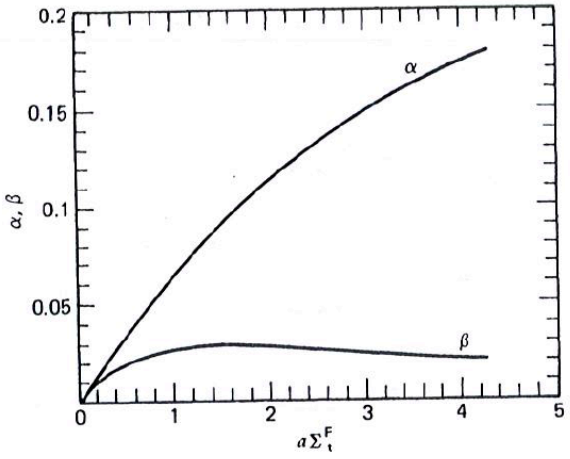


Figure 3: Parameters used in ABH method. [5]

To confirm the results from the ABH method, Monte-Carlo N-Particle (MCNP) software code developed at Los Alamos National Laboratory is also utilized to determine the reactivity effects of the coatings on a fuel pin. The MCNP code can be used for particle transport and for eigenvalue calculations (e.g. k_{eff}) for numerous scenarios. In this study, a single, one-dimensional fuel rod (infinite in length) is used with five regions: fuel, gap, cladding, film, and

moderator. Within MCNP, the KCODE card is implemented to solve for the k_{eff} eigenvalue (example problem in Appendix). [7]

2.2: Fuel Cycle Length

To approximate the impact on isotope depletion, the production chains for the principal isotopes (e.g. = Uranium 235), neutron flux, and reactivity calculations must be coupled. A variation in reactivity due to the film will directly affect the refueling schedule of the reactor. Thus, it is vital to evaluate the impact on the fuel cycle length in order to examine the economic performance of a reactor. In order to assess fuel burnup and loss in fuel cycle length a linear reactivity model is used to estimate impact of changes in initial reactivity on burnup. Reactivity (ρ) loss as a function of burnup (B) becomes fairly linear after a few months of operation for a reactor, as is illustrated by Figure 4. [8]

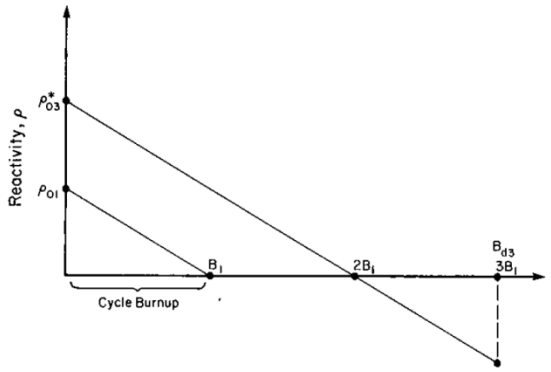


Figure 4: Linear Relationship of reactivity and burnup at a nominal initial reactivity. [8]

The change in reactivity previously obtained using the ABH method and MCNP can be used to approximate the burnup of the fuel. That is, one can multiply the percent loss in reactivity by an

initial fuel cycle length value. Figure 5 from the *Linear Reactivity Model for Nuclear Fuel Management* text illustrates the linear estimate using a 300 days fuel cycle at 4.34 wt.% enrichment supplied via Electric Power Research Institute (EPRI) [8].

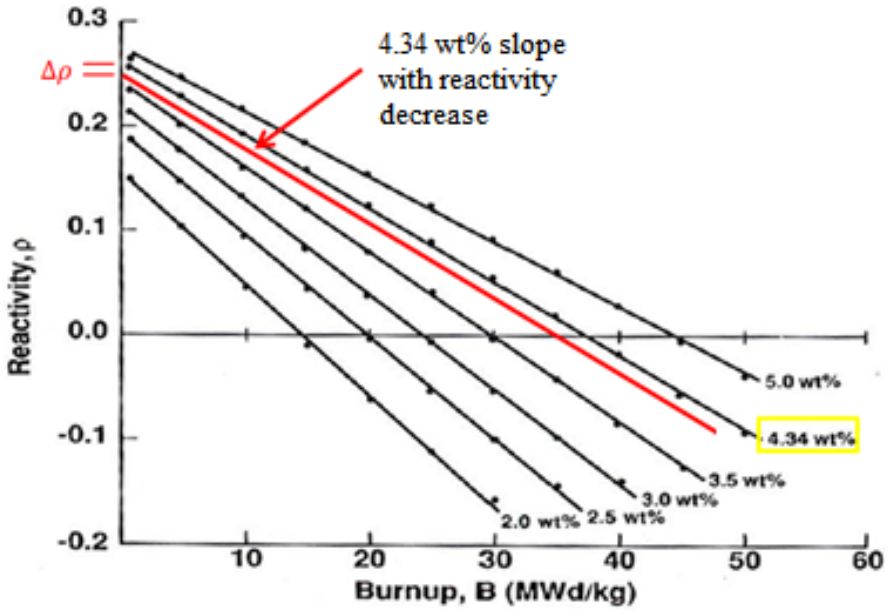


Figure 5: Reactivity vs. Burnup relationship obtained from the EPRI. [8]

The red-line in Figure 5 is added to illustrate the change in reactivity and the impact on the burnup for a reference reactor. In this study, this linear reactivity model is used to assess the loss in fuel cycle length for a 900 day cycle (i.e. three periods of 300 days within the reactor) and the final burnup value based on a reference burnup of 50 MWd/kg. The loss in fuel cycle length (days) and final burnup value is obtained from the reactivity change from a regular (no-film region) fuel pin.

2.3: One-Dimensional Fuel Temperature

The addition of a ceramic film will affect the heat transfer between the fuel and moderator, thus changing the maximum fuel temperature. It is crucial to verify that the maximum fuel temperature, or in this case the fuel centerline temperature, remains within a safe region. In this study, the overall thermal resistance of a fuel pin is used to evaluate the temperature drop from the fuel centerline to the coolant. This task can be accomplished by using a circuit analogy of a series of thermal resistances for each region: fuel, gap, cladding, ceramic film, and coolant. Figure 6 from Todreas illustrates the temperature profile for the five regions: [6]

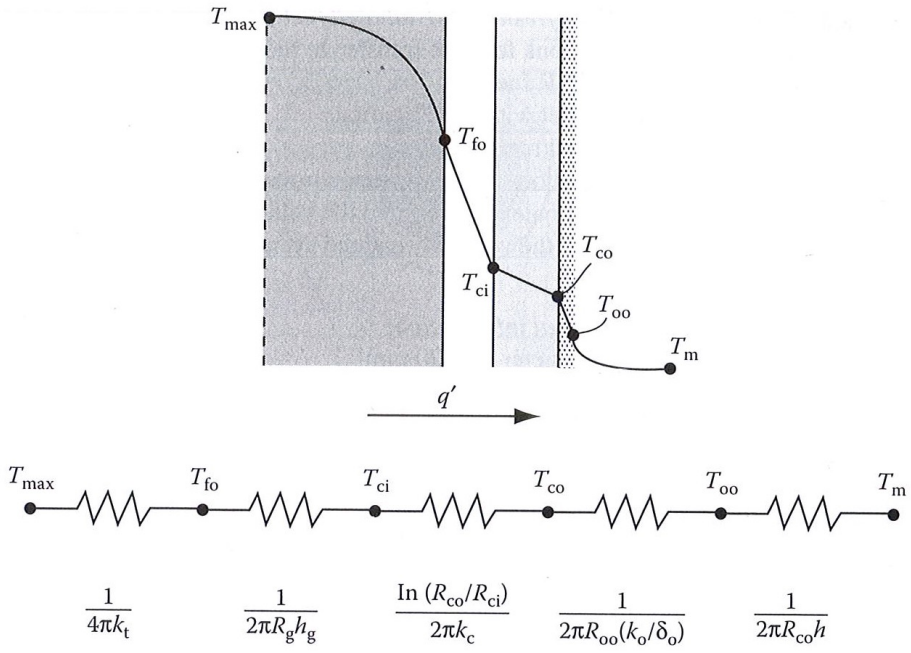


Figure 6: Electrical circuit analogy for thermal resistance across a cylindrical fuel pin. [6]

where $T_{\max}$ (or T_{CL}) is the centerline temperature, T_{fo} is the outer surface temperature of the fuel, T_{ci} is the inside surface cladding temperature, T_{co} is the outer surface temperature of the cladding, T_{oo} is the outer ceramic film temperature, and T_{m} is the moderator temperature.

Now, we must derive the unique heat transfer equations for each region. Starting in the fuel region, the heat conduction equation for a cylindrical fuel pellet with a uniform volumetric heat source (q''') and ignoring axial heat conduction takes the form: [5,6]

$$\frac{1}{r}\frac{d}{dr}k_{\mathrm{F}}\,r\frac{dT}{dr} = -q''' \qquad \text{(Eq.16)}$$

where r is the position radius, k_{F} is the thermal conductivity of the fuel, and T is temperature. To simplify the equation, we consider a constant thermal conductivity and no dependency on position or temperature, thus $\frac{d}{dr}k_{\mathrm{F}} = 0$. Now we are able to solve for the temperature drop across the fuel pin (dT/dr): [6]

$$\frac{dT}{dr} = T_{\mathrm{CL}} - \frac{q'''r^2}{4\,\overline{k_{\mathrm{F}}}}\,. \qquad \text{(Eq.17)}$$

We can define this function in terms of linear power density (q'), yielding a new form of the previous equation:

$$q' = \pi r_{\mathrm{F}}^2 q''' \qquad \text{(Eq.18)}$$

$$\Delta T_{\mathrm{F}} = \frac{q'}{4\pi\,\overline{k_{\mathrm{F}}}} \qquad \text{(Eq.19)}$$

Note that this form is based on the assumption that fuel temperature is only dependent on the fuel's thermal conductivity and the linear power density, and not the fuel radius. [5,6]

Second region is the gap between the fuel pellet and the cladding. This region has a tight clearance between the fuel and cladding with values around 0.008 cm and usually filled with an inert gas (e.g. helium) for LWRs. [5] Without going through a full derivation of the heat

equation, similar to the equation for the fuel region (except no heat production), we can show the final form of the equation for the temperature drop across the gap as: [5,6]

$$\Delta T_{\mathrm{G}} = \frac{q''}{h_{\mathrm{G}}} \qquad \text{(Eq.20)}$$

where, h_{G} is the heat transfer coefficient in the gap region and the heat flux (q'') across the gap region is the amount of heat produced from the fuel divided by the surface area of the fuel region. That is, in terms of heat flux, the equation takes the form:

$$q'' = \frac{q'''(\pi r_{\mathrm{G}}^2 H)}{2\pi r_{\mathrm{G}} H} = \frac{q''' r_{\mathrm{G}}}{2} = \frac{q'}{2\pi r_{\mathrm{G}}} \ , \qquad \text{(Eq.21)}$$

then combining the equations to obtain the final equation for temperature drop across the gap: [5,6]

$$\Delta T_{\mathrm{G}} = \frac{q''' r_{\mathrm{G}}}{2h_{\mathrm{G}}} = \frac{q'}{2\pi r_{\mathrm{G}} h_{\mathrm{G}}} \, . \qquad \text{(Eq.22)}$$

The third region of the fuel pin is the cladding. This region, like the gap, has no heat production term, thus we are able to solve the temperature drop fairly easily. The heat conduction equation takes the form [6]

$$\frac{1}{r}\frac{d}{dr} k_{\mathrm{C}} \, r \frac{dT}{dr} = 0 \, . \qquad \text{(Eq.23)}$$

Sparing the details, we are able to find the temperature drop across the clad: [5,6]

$$\Delta T_{\mathrm{C}} = \frac{q''' r_{\mathrm{C}}}{2} \frac{t_{\mathrm{C}}}{k_{\mathrm{C}}} = \frac{q'}{2\pi \, r_{\mathrm{C}}} \frac{t_{\mathrm{C}}}{k_{\mathrm{C}}} \ , \qquad \text{(Eq.24)}$$

where k_{C} represents the thermal conductivity of the clad and t_{C} is the clad thickness.

The fourth region is the ceramic film. The temperature drop across the film, like the gap and cladding, is dependent on the thermal conductivity and the thickness of the film. Assuming no heat production from the film, the heat conductivity equation can be solved to obtain a temperature profile across the film: [6]

$$\Delta T_{film} = q'' \frac{t_{film}}{k_{film}} = \frac{q'}{2\pi} \frac{t_{film}}{r_{film}\, k_{film}}, \qquad \text{(Eq.25)}$$

where t_{film} is the film thickness, r_{film} is the distance to the outside of the film, and k_{film} is the thermal conductivity of the film region.

The last region is the moderator region. The heat flux leaving the fuel pin and emerging into the moderator region is given by:

$$q''_{pin} = h_s\left(T_{film} - T_{\mathrm{M}}\right), \qquad \text{(Eq.26)}$$

where h_s is the heat transfer coefficient between the film-moderator region (dependent on flow conditions), T_{film} is the outer temperature of the ceramic film, and T_{M} is the moderator temperature. The temperature drop from the film to the moderator is obtained by solving the previous equation for $T_{film} - T_{\mathrm{M}}$:

$$T_{film} - T_{\mathrm{M}} = \frac{q''}{h_s} = \frac{r_{fuel}^2\, q'''}{h_s\, 2r_{film}} = \frac{q'}{2\pi\, r_{film} h_s} \ . \qquad \text{(Eq.27)}$$

Note that normal notation for uses the difference between surface temperature and the coolant/moderator temperature. In this case, the film's outer surface is the surface temperature. Now the overall thermal resistance equation can be found by adding each of the regions: [5,6]

$$T_{\mathrm{CL}} - T_{\mathrm{M}} = \frac{q'}{2\pi}\left(\frac{1}{2k_{Fuel}} + \frac{1}{r_g h_g} + \frac{t_{\mathrm{C}}}{r_{\mathrm{C}} k_{\mathrm{C}}} + \frac{t_{film}}{r_{film}\, k_{film}} + \frac{1}{r_{film} h_s}\right) . \qquad \text{(Eq.28)}$$

The linear power density and moderator/coolant temperature will change along the length of the channel. We can assume that the linear power density has a sine-like shape along the length of the flow channel: [5]

$$q'(z) = q_0' \sin\left(\frac{\pi z}{H}\right). \qquad \text{(Eq.29)}$$

Then we can compute the coolant temperature along the channel by using a simple energy balance equation gained by the coolant from the fuel:

$$w c_{\mathrm{p}} dT = q''(2\pi r_F) dz = q'(z) dz \qquad \text{(Eq.30)}$$

where w is the mass flow, c_{p} is the specific heat of the coolant, and z is the position along the channel. Using this form, we can integrate the up the flow channel from inlet to outlet (temperature and position): [5]

$$w c_{\mathrm{p}} \int_{T_{inlet}}^{T_{\mathrm{M}}} dT = q_0' \int_0^z dz' \sin\left(\frac{\pi z'}{H}\right) . \qquad \text{(Eq.31)}$$

Solving this equation, we can calculate the temperature of the coolant at position z along the channel: [5]

$$T_{\mathrm{M}}(z) - T_{inlet} = \frac{q_0' H}{\pi c_{\mathrm{p}} w}\left[1 - \cos\left(\frac{\pi z}{H}\right)\right] . \qquad \text{(Eq.32)}$$

Inserting the position dependent linear power density and moderator temperature into the overall thermal resistance equation: [5,6]

$$T_{\mathrm{CL}} = T_{inlet} + \frac{q_0' H}{\pi \mathrm{c_p} w}\left[1 - \cos\left(\frac{\pi z}{H}\right)\right] + \frac{q_0' \sin\left(\frac{\pi z}{H}\right)}{2\pi}\left(\frac{1}{2k_{Fuel}} + \frac{1}{r_g h_g} + \frac{t_{\mathrm{C}}}{r_{\mathrm{C}} k_{\mathrm{C}}} + \frac{t_{film}}{r_{film}\, k_{film}} + \frac{1}{r_{film} h_s}\right). \quad \text{(Eq.33)}$$

Each of the proposed films will have a unique thermal conductivity, thus each film will affect the system uniquely, along with any film thickness variation (i.e. r_{film} , t_{film} , k_{film}).

2.4: Film Roughness

To further assess the impact the ceramic film yields on the system, the roughness of the film itself must be considered. This roughness, or friction, between the film-moderator will affect the heat transferred between the pin and the moderator, as well as present a pressure drop along the flow channel. [9] In order to evaluate the change in the heat transfer coefficient (h) and the pressure drop, the Moody diagram is used to obtain the Darcy friction factor (f) for various experimental roughness values. The Moody diagram relates flow parameters (e.g. Reynolds number, Re) and the roughness of the material to the Darcy friction factor. The Darcy friction factor is used in fluid dynamics to relate pressure drop produced by the friction between the wall of a pipe and the fluid flow. [6,9]

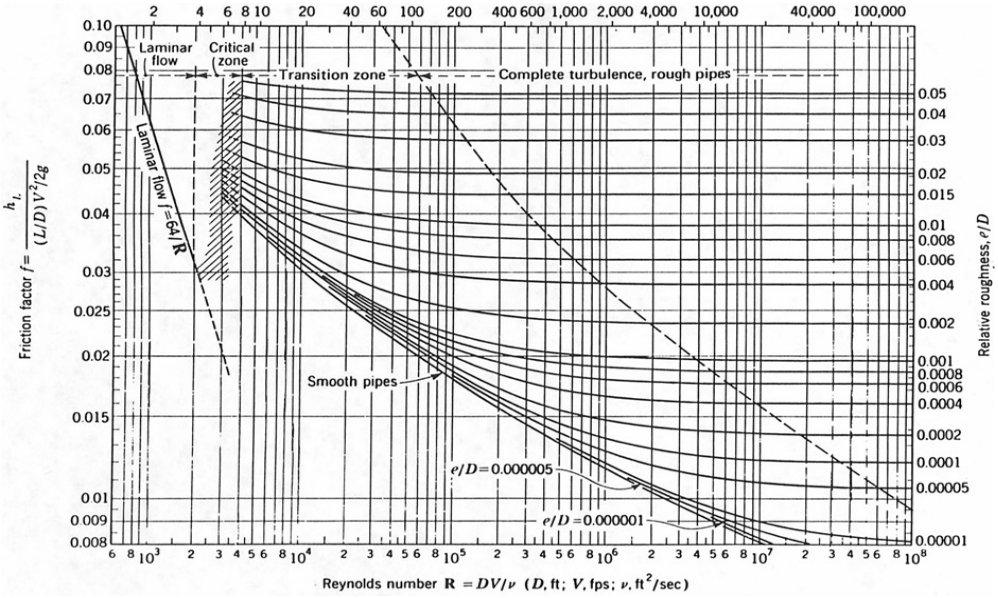


Figure 7: Moody diagram illustrating relationship between friction factor, relative surface roughness, and flow parameters. [9]

The relative roughness is defined as the average roughness divided by the diameter of the cylinder. The average roughness used in this study is the *arithmetic average of absolute values*, denoted as R_a. [9] The actual values for the films' roughness will be discussed later.

The roughness of film will produce a head loss due to the friction effects along the wall, or in our case, the outside of the fuel pin. Along the flow channel, the film induces a shear stress on the flow which decreases the fluid motion. [9] For steady-state, steady-flow conditions, the energy equation of the fluid can be written as

$$\frac{P_1}{\rho g} + \frac{v_1^2}{2g} + z_1 = \frac{P_2}{\rho g} + \frac{v_2^2}{2g} + z_2 + h_f \,, \qquad \text{(Eq.34)}$$

where the subscript denotes the position along the cylindrical channel, P is pressure, ρ is the density of the fluid, v is the flow velocity, g is gravity, z is position along the channel, and h_f is the head loss due to wall friction. Solving this equation for a given channel length L and same

flow velocity along the channel, we can obtain an equation for pressure loss as a function of the Darcy friction factor:

$$\Delta P = \rho \mathrm{g} \left[f \frac{\mathrm{L}}{\mathrm{d_h}} \frac{v^2}{2\mathrm{g}} \right] \quad \text{(Eq.35)}$$

where $\mathrm{d_h}$ represents the hydraulic diameter. [6,9]

With the aim of evaluating the impact on the heat transfer coefficient the film roughness introduces, the Prandtl and Nusselt number are required. The Prandtl (Pr) number is the ratio of molecular diffusivity of momentum to that of heat in the fluid and is required to obtain the Nusselt number. The Nusselt (Nu) number expresses the ratio of convection to conduction heat transfer across a boundary. The equations for Pr and Nu are as follows:

$$\mathrm{Pr} = \frac{\mu \, c_p}{k} \quad \text{(Eq.36)}$$

where, μ is the dynamic viscosity, c_p is the specific heat, and k is the thermal conductivity of the fluid;

$$\mathrm{Nu} = \frac{h \, \mathrm{d_h}}{k} \quad \text{(Eq.37)}$$

where, h is the heat transfer coefficient. [9]

In order to evaluate the film's roughness impact directly, an alternate form of the Nusselt number is obtained using the Darcy friction factor. A correction by Gnielinski is given to correlate turbulent flow in tubes between the Reynolds (Re) number, Prandtl (Pr) number, and friction factor (f) is given: [6]

$$\mathrm{Nu} = \frac{(f/8)\mathrm{Re}*\mathrm{Pr}}{1+12.7\sqrt{f/8}\left(\mathrm{Pr}^{2/3}-1\right)} . \quad \text{(Eq.38)}$$

The *Gnielinski correlation* is valid for: [9]

$$0.5 \leq \mathrm{Pr} \leq 2000$$
$$3000 \leq \mathrm{Re} \leq 5E6 .$$

Now, one is able to obtain a value for the heat transfer coefficient by solving the original Nusselt equation:

$$h = \frac{\mathrm{Nu}\ k}{\mathrm{d_h}} . \quad \text{(Eq.39)}$$

This study will evaluate the change in the heat transfer coefficient under various flow conditions and several roughness values.

2.5: Uncertainty Analysis

To obtain more knowledge regarding the impact the film presents on the system, uncertainty analysis is vital. The uncertainty in these calculations arises due to lack of knowledge in certain parameters. In this study, the uncertainty of the ABH method used to evaluate the thermal utilization and the temperature change across a fuel pin are analyzed. For each of the respective equations, the variables where the uncertainty is addressed are as follows:

ABH Method: P_{FO} (first-flight escape probability) and $\Sigma_{abs}^{\mathrm{M}}$

Temperature Change: h_{s} (heat transfer coeff. between film-moderator) and k_{film}

Regarding the ABH method parameters, the first-flight escape probability expresses the probability that a neutron born in the fuel will make its next collision in the moderator. With the of a ceramic film, the probability should decrease due to the film introducing its own probability of collision. The moderator's absorption cross-section is lumped with the film's volume-weighted absorption cross-section. Coupling this parameter with a certain uncertainty illustrates the impact the film might introduce.

For the temperature calculation, the heat transfer coefficient between the coolant-film and the (approximated) thermal conductivity of the film are both given values of uncertainty due to lack of information and author's estimations for both parameters.

For the above parameters, a triangular distribution model is used to exhibit the variability. In order to properly assess the lowest, highest, and peak values for the triangular model, estimated perturbations are used with respect to each variable. The perturbation values will be discussed later within the *Results* section.

Using the probability distributions to obtain the lowest and highest values in the triangular distribution, Monte Carlo techniques are employed to acquire values from each of the probability functions. Monte Carlo sampling relies on repeated random sampling from these inputted triangular distributions resulting in a converged solution. *@Risk* software is implemented to analyze both temperature change and the ABH method for the given input distributions. This software performs risk analysis using Monte Carlo simulations within Microsoft Excel. By running the simulation numerous times (e.g. $1E6$ histories), an output distribution of solutions is obtained. [10]

In order to properly assess the lowest, highest, and peak values for the triangular model, estimated perturbations are used with respect to each variable.

ABH Method:

P_{FO} with 10% perturbation

$\Sigma_{abs}^{\mathrm{M}}$ with 20% perturbation

Centerline Temperature:

h_{s} with 15% perturbation

k_{film} with 20% perturbation

Table 1 contains numerical values of the uncertainty using ZrO_2 film.

Table 1: Triangular Distribution Parameters for an example uncertainty values for ZrO_2 film.

	ABH Method		Centerline Temperature	
Parameter	P_{FO}	$\Sigma_{\mathrm{abs}}^{\mathrm{Mod}\ *}$	h_s	$k_{film}{}^{*}$
Minimum	0.4	0.16	2.4	1.6
Most Likely	0.5	0.22	3.0	2.0
Maximum	0.6	0.28	3.6	2.4

The asterisks on the macroscopic absorption cross-section and the thermal conductivity of the film in Table 1 indicate the parameters will change for each film. Furthermore, the film's thickness will also impact the moderator absorption cross section (i.e. film's cross section is added to the moderator region). Figures 8 and 9 illustrate the basic methodology for the Monte Carlo simulations for the ABH method and the fuel centerline temperature, respectively, with an example reference output from *@Risk*.

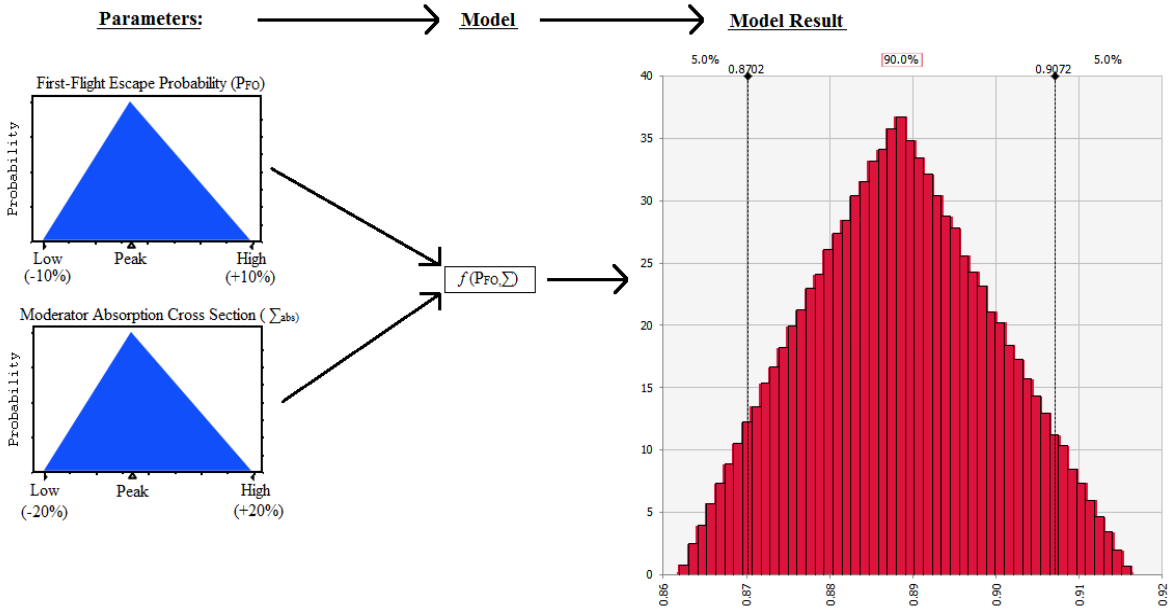


Figure 8: Flow of a Monte Carlo simulation for ABH method to calculate the thermal utilization factor.

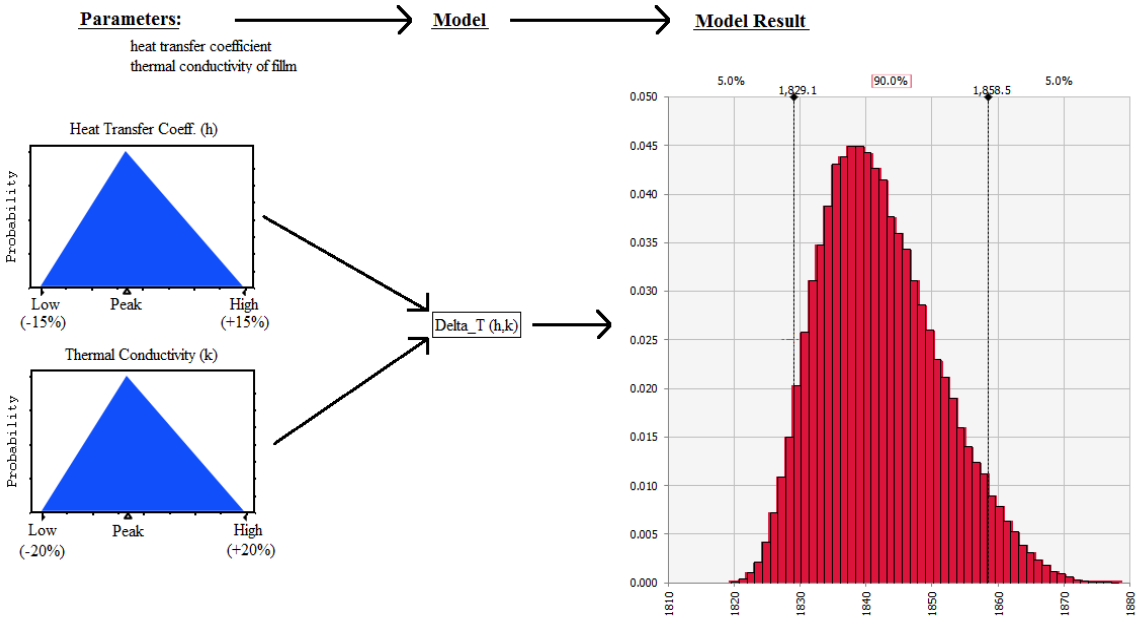


Figure 9: Monte Carlo simulation for fuel temperature calculation for the heat transfer coefficient and thermal conductivity of the film.

To verify the results from *@Risk*, MATLAB is used. Employing the previous MATLAB codes used to calculate the thermal utilization (ABH method) and temperature change, the probability functions are entered for each of the parameters, respectively. The calculations result in a distribution of solutions with a computed variance and standard deviation.

2.6: Fuel and Coolant Temperature during Transients

Using the overall thermal resistance equation, we can set a time dependent equation for various parameters in order to understand how the film will impact certain transient conditions. This study evaluates variable flow and variable (linear) power density while retaining a predetermined moderator temperature change (ΔT_{M}) along the channel. Both time dependent equations are given an exponential decay. For this analysis, the values (i.e. flow rate and power density) are decreased exponentially to one-half of the original value. The general form for a given function $f(t)$ is given by:

$$f(t) = \tfrac{1}{2} f(0)[\exp(-\lambda\, t) + 1] \quad , \tag{Eq.39}$$

where t is response time and λ is a value given to the slope of change (i.e. how quickly the exponential change will occur, or exponential decay value). Using the two parameters we wish to assess, two equations are formed with the same form:

$$q'(t) = \tfrac{1}{2} q'(0)[\exp(-\lambda_1 t) + 1] \ , \tag{Eq.40}$$

$$v(t) = \tfrac{1}{2} v(0)[\exp(-\lambda_2 t) + 1] \ . \tag{Eq.41}$$

Thus, the product of the eigenvalue and time yield the response time of the varying parameter. That is, by varying the mass flow faster than the linear power density (i.e. $\lambda_2 > \lambda_1$) will produce a momentary increase in coolant temperature. In this study, both mass flow and linear power density are varied by unique values ($\lambda_{1,2}$) and compared to changes in a regular (no-film) fuel pin. For example, by assuming the exponential term is equal to a value, on can solve for the decay constant.

$$\mathrm{R}_{1,2} = \exp\left(-\lambda_{1,2}\, t\right), \tag{Eq.42}$$

One can obtain an equation for $\lambda_{1,2}$:

$$\lambda_1 = \frac{\ln \mathrm{R}_1}{t_1}, \tag{Eq.43}$$

$$\lambda_2 = \frac{\ln \mathrm{R}_2}{t_2}, \tag{Eq.44}$$

where $t_{1,2}$ represent the response times and $\mathrm{R}_{1,2}$ yield the slope of the exponential decay for each equation, respectively. In this study we use response time values ($t_{1,2}$) of 60 seconds and 25 seconds with identical $\mathrm{R}_{1,2}$ values set to 0.5.

The flow velocity directly impacts the mass flow of the flow channel. This expression is given by:

$$\dot{m}(t) = v(t) A_{cs} \rho\,, \tag{Eq.45}$$

for A_{cs} is the cross-sectional area of the channel with a moderator density of ρ.

Combining the two time-dependent equations with the thermal resistance equation, we obtain:

$$T_{\mathrm{CL}} = T_{inlet} + \frac{\left(\frac{1}{2}q'(0)[\exp(-\lambda_1 t)+1]\right)H}{\pi \mathrm{c_p} \dot{m}(t)}\left[1-\cos\left(\frac{\pi z}{H}\right)\right] + \frac{\left(\frac{1}{2}q'(0)[\exp(-\lambda_1 t)+1]\right)\sin\left(\frac{\pi z}{H}\right)}{2\pi}\left(\frac{1}{2k_{Fuel}} + \frac{1}{R_g h_g} + \cdots\right.$$

$$\left.\frac{1}{k_{Clad}}\ln\left(\frac{R_{co}}{R_{ci}}\right) + \frac{\delta_o}{R_{oo}k_{film}} + \frac{1}{R_{oo}h}\right) \quad . \qquad \text{(Eq.46)}$$

This equation is implemented using MATLAB software for all proposed films and compared with a reference, no-film pin.

3: Results

3.1: Reactivity Impact

Several parameters in the final expression of the ABH method previously derived are changed due to the addition of a coating. The addition of the coating region will slightly lower the moderator volume (dependent on film thickness), consequently decreasing the moderator-to-fuel volume fraction $\left(\frac{V_{\mathrm{M}}}{V_{\mathrm{F}}}\right)$ slightly (~0.40% decrease for 10 micron film). The volume of the moderator is obtained via subtracting the fuel, gap, clad, and film volumes from the squared pitch. If we assume a one centimeter depth, we can use the cross sectional areas to obtain a volume for each region. That is,

$$\text{Area total} = \text{Pitch}^2 = \pi \mathrm{r}_{\mathrm{M}}^2 \qquad \text{(Eq.47)}$$

then moderator volume-fraction can be obtained by

$$V_{\mathrm{M}}^* = \frac{\text{Pitch}^2 - \pi\left(\mathrm{r}_{\mathrm{F}}+\mathrm{r}_{\mathrm{gap}}+\mathrm{r}_{\mathrm{clad}}+\mathrm{r}_{\mathrm{film}}\right)^2}{\text{Pitch}^2} \ , \qquad \text{(Eq.48)}$$

where $\mathrm{r}_{\mathrm{F}}, \mathrm{r}_{\mathrm{gap}}, \mathrm{r}_{\mathrm{clad}}, \text{and } \mathrm{r}_{\mathrm{film}}$ are the radius values to the fuel, gap, clad and film region, respectively (the asterisk* on the moderator volume indicates the new value due to the film region).

The film will also introduce a higher absorption rate outside of the fuel region; therefore the absorption cross-section of the film is combined with the moderator cross section in the ABH equation. The cross section of the film is volume-averaged with the moderator cross section to obtain a new overall moderator absorption cross-section. The new moderator cross-section and new fuel diameter impact the lattice function through the L_{M} variable (i.e. recall, $L_{\mathrm{M}} = D_{\mathrm{M}}/\Sigma_{abs}^{\mathrm{M}}$)

and the fuel boundary condition (a), see Figure 3. The new moderator cross section takes the form of

$$\Sigma_{abs}^{\mathrm{M}^*} = \left(\frac{V_{\mathrm{M}}}{V_{\mathrm{M}}+V_{\mathrm{film}}}\right)\Sigma_{abs}^{\mathrm{M}} + \left(\frac{V_{\mathrm{film}}}{V_{\mathrm{M}}+V_{\mathrm{film}}}\right)\Sigma_{abs}^{\mathrm{film}} \ . \qquad \text{(Eq.49)}$$

The final expression of the ABH method with the film present is shown where each parameter that is affected is given an asterisk $(*)$:

$$\frac{1}{f} = \frac{\boldsymbol{\Sigma_{abs}^{\mathrm{M}^*}V_{\mathrm{M}}^*}}{\Sigma_{abs}^{\mathrm{F}}V_{\mathrm{F}}}\left\{1 + \frac{\Sigma_{abs}^{\mathrm{F}}}{\Sigma_{tot}^{\mathrm{F}}}\left[\frac{1-P_{\mathrm{FO}}}{P_{\mathrm{FO}}} - \boldsymbol{a}^*\Sigma_{tot}^{\mathrm{F}}\right]\left[1 + \alpha\left(\frac{\Sigma_s^{\mathrm{F}}}{\Sigma_{tot}^{\mathrm{F}}}\right) + \beta\left(\frac{\Sigma_s^{\mathrm{F}}}{\Sigma_{tot}^{\mathrm{F}}}\right)^2\right]\right\} + \left(\frac{\boldsymbol{a}^* d}{2\boldsymbol{L_{\mathrm{M}}^{2}}^*} - \boldsymbol{a}^*\boldsymbol{\Sigma_{abs}^{\mathrm{M}^*}}\right)\left(\frac{\boldsymbol{V_{\mathrm{M}}^*}}{V_{\mathrm{F}}}\right) + E\left(\frac{\boldsymbol{a}^*}{\boldsymbol{L_{\mathrm{M}}^*}}, \frac{b}{\boldsymbol{L_{\mathrm{M}}^*}}\right) \ . \qquad \text{(Eq.50)}$$

This study assesses a Westinghouse PWR with the fuel pin dimensions summarized in 2. [5]

Table 2: Geometric parameters of reference fuel pin and coating.

Parameter	Variable	Value
Fuel Radius	$\mathrm{r_{fuel}}$	0.4095 cm
Gap Thickness	$\mathrm{t_{gap}}$	0.0082 cm
Clad Thickness	$\mathrm{t_{clad}}$	0.0572 cm
Coating Thickness	$\mathrm{t_{film}}$	5 or 10 micron
Fuel Element Pitch	Pitch	1.25 cm

Next, the absorption cross section for each film is required. The absorption macroscopic cross section is evaluated in Equation 50:

$$\Sigma_{abs} = \mathrm{N}\sigma_{abs} \qquad \text{(Eq.51)}$$

where, N represents the number density and σ_{abs} is the absorption microscopic cross section.

The number density, represented in Equation 51, represents the number of atoms per volume:

$$N = \frac{\rho * N_{AV}}{M} \quad \text{(Eq.52)}$$

where, ρ is the film density, N_{AV} is Avogadro's number, and M is the molecular weight. The required data to obtain the macroscopic cross section for each film is presented in Table 3. [11,12,13]

Table 3: Film properties.

Film	σ_{abs} (b)	Atomic Weight (g/mole)	Density (g/cc)
TiAlN	7.921	88.888	3.86
ZrO_2	0.1854	123.22	6.00
Ti_2AlC	11.845	134.791	4.10
Ti_3AlC_2	17.649	194.702	2.93

Using these equations, the macroscopic absorption cross section (i.e. for (n, γ) reactions) can be obtained for each film.

Table 4: Absorption cross section for proposed ceramic films.

Film	Σ_{abs} (cm^{-1})
TiAlN	0.2074
ZrO_2	0.0054
Ti_2AlC	0.1180
Ti_3AlC_2	0.1601

To calculate the thermal utilization from the ABH method, MATLAB program is implemented to acquire values for each film, as well as a reference, no-film pin. The percent change from the reference is shown in Table 5 (See Appendix for MATLAB code).

Table 5: Analysis of 5 micron and 10 micron thick film region with the ABH method.

Simulation	Film Thickness (micron)	Thermal Utilization	% Change
Reference	-	0.8847	-
ZrO_2	5	0.8844	0.03%
TiAlN	5	0.8832	0.14%
Ti_2AlC	5	0.8833	0.15%
Ti_3AlC_2	5	0.8837	0.11%
ZrO_2	10	0.8842	0.05%
TiAlN	10	0.8821	0.27%
Ti_2AlC	10	0.8820	0.30%
Ti_3AlC_2	10	0.8827	0.22%

The change differs for each film due to unique values of density, which in return affects the absorption macroscopic cross section (i.e. through the number density) and the film's microscopic absorption cross section. To compare as well as validate the change in reactivity via the ABH method, MCNP code is implemented. Using an infinite cylinder (i.e. infinite in length/height), a multiplication factor was calculated for each film as well as a reference fuel pin (See Appendix for MCNP input deck). A single fuel pin is used in the MCNP geometry with white boundaries on the outer boundary of the moderator. The multiplication factor (KCODE) calculation is performed using 1000 cycles and 1000 histories per cycle. The output k-value from MCNP is shown in Table 6 together with the previous ABH method values.

Table 6: Reactivity impact from 5 and 10 micron thick film.

Simulation	Thickness (micron)	MCNP		ABH Method
		***k*-value**	**% change**	**% change**
Reference	-	1.49032	-	-
ZrO_2	5	1.48961	0.05%	0.03%
TiAlN	5	1.48768	0.18%	0.14%
Ti_2AlC	5	1.48879	0.10%	0.15%
Ti_3AlC_2	5	1.48948	0.06%	0.11%
ZrO_2	10	1.48936	0.06%	0.05%
TiAlN	10	1.48741	0.20%	0.27%
Ti_2AlC	10	1.48654	0.25%	0.30%
Ti_3AlC_2	10	1.48716	0.21%	0.22%

The k_{eff} values are well above the typical 1.0 values due to the white boundary inputted within MCNP. That is, the neutrons are reflected on the outside of the moderator region boundary, thus increasing the probability of being absorbed back in the fuel. Additionally, these calculations are coupled with a corresponding uncertainty analysis.

3.2: Loss in Fuel Cycle Length

The change in reactivity (or k_{eff}) is used to approximate the impact on the fuel cycle length via the linear reactivity model. To assess the change in fuel cycle length, the reactivity change obtained from the MCNP simulations is used to estimate the loss in fuel cycle length and total burnup of the fuel. In this study, it is assumed a fuel element is in the reactor for three cycles of 300 days (i.e. 900 days total) and a reference burnup value of $50\ \text{MWd/kg}$ is used, where a

decrease in reactivity will directly impact the fuel cycle length. The loss in days of the fuel cycle and the corresponding burnup is presented in Table 7.

Table 7: Estimated loss fuel cycle length based on a 900 day cycle and fuel burnup.

Film	Thickness (micron)	Reactivity Change (MCNP)	Cycle Loss Estimate (days)	Burnup (MWd/kg)
ZrO_2	5	0.05%	0.45	48.6
TiAlN	5	0.18%	1.62	48.5
Ti_2AlC	5	0.10%	0.90	48.6
Ti_3AlC_2	5	0.06%	0.54	48.6
ZrO_2	10	0.06%	0.54	48.5
TiAlN	10	0.20%	1.80	48.5
Ti_2AlC	10	0.25%	2.25	48.4
Ti_3AlC_2	10	0.21%	1.89	48.5

The fuel length impact may be of primary interest for utilities, due to the reactor not creating power and to increasing the rate of refueling. In order to achieve the same fuel cycle, the fuel enrichment can be increased. For the 10 micron thick films, the fuel cycle impact is over two days for three of the films ($TiAlN, Ti_2AlC, Ti_3AlC_2$), with largest fuel cycle loss of 2 days for the 10 micron Ti_2AlC which may be of concern. The films decrease the total burnup to around 48.5 MWd/kg, a decrease of 1.5 MWd/kg from the reference case from the text at 4.34 wt%. [8]

3.3: Fuel Maximum Temperature

Adding coatings to the fuel pin should increase the fuel centerline temperature by increasing the thermal conduction path a small amount; however, they may have a higher heat transfer coefficient than the cladding and consequently lower the fuel centerline temperature. A rough estimate of this change is obtained based on typical PWR values listed in Tables 8 and on

estimates for thermal conductivities listed in Table 9. [5,11,12,13] It should be noted that in this study the maximum linear power density is used to validate that the fuel will remain in a safe temperature region.

Table 8: Parameters for the calculation of temperature changes in a fuel pin.

Parameter	Variable	Value
Linear Power Density (*Maximum*)	$q'_{\max}$	460 W/cm
UO_2 Fuel Thermal Conductivity	k_{Fuel}	0.0250 W/cm-K
Clad (Zircaloy IV) Conductivity	k_{Clad}	0.1070 W/cm-K
Heat transfer coefficient in gap	h_{Gap}	0.75 W/cm^2-K
Heat transfer coefficient in moderator	h	3.0 W/cm^2-K
Inlet Moderator Temperature	T_{Mod}	290°C

Table 9: Thermal conductivity of proposed coatings.

Coating	Thermal Conductivity (W/m-K)
ZrO_2	2.0
TiAlN	5.0
Ti_2AlC	30.0
Ti_3AlC_2	40.0

The thermal conductivity characterizes the film's ability to transfer heat. That is, a smaller thermal conductivity yields a lower heat transfer rate through the film; thus, resulting in a higher fuel temperature compared to the high thermal conductivity films. Using the thermal resistance equation previously derived, the change in the maximum temperature can be calculated.

Table 10: Impact on fuel centerline temperature for each film at 5 and 10-micron thickness.

Film	**Thickness** (micron)	**Centerline Temperature** (°C)	**Change in T_{CL}** (%)
Reference	-	1834.80	-
ZrO_2	5	1840.89	0.33%
TiAlN	5	1837.22	0.13%
Ti_2AlC	5	1835.18	0.02%
Ti_3AlC_2	5	1835.07	0.02%
ZrO_2	10	1847.01	0.67%
TiAlN	10	1839.66	0.27%
Ti_2AlC	10	1835.58	0.04%
Ti_3AlC_2	10	1835.38	0.03%

The centerline temperature is constrained to remain below the melting temperature of the fuel ($\sim$2800°C), [5] and the calculated fuel centerline temperatures for each simulation are well below the melting point of the fuel. This study used a one-dimensional thermal analysis, thus neglecting any axial conductance, as well as analyzing only a single fuel pin. The significance of these simulations is the percent changes each film introduces on the centerline temperature. Due to the small thickness values proposed of 5 and 10-microns coupled with a low thermal conductivity film introduces a slight increase with the largest increase in temperature (10-micron ZrO_2 film) from the reference is 0.67% (12.21°C).

3.4: Film Roughness Impact

To illustrate the impact the film's roughness presents on the system, change in the heat transfer coefficient is analyzed under normal flow parameters. For reference and comparison, typical heat

transfer coefficient values for Zr-clad to Water ranges from $2.8 - 4.5 \frac{\mathrm{W}}{\mathrm{cm^2\ K}}$ depending on flow parameters, as seen in Table 11. [5,6]

Table 11: Physical properties of water coolant. [5]

Coolant	$\mathbf{T_{inlet}}$ (°C)	$\mathbf{\Delta T}$ (°C)	Pressure (bar)	$\mathbf{\Delta P_{core}}$ (bar)	$\overline{v}_z$ (cm/s)	Density (g/cc)	h_s ($\mathrm{W/cm^2K}$)
H_2O	300	20	100	2	400	0.7	2.8-4.5

For the currently proposed films, roughness values (Ra) of around 10μin (0.25 microns) for the 5 and 10-micron thick films have been deposited in experiments. [14] This value is used with two perturbations of 50% decrease (5μin) and a 50% increase (15μin) in roughness to illustrate the change on the heat transfer coefficient. We assume a typical flow velocity of $4.0\ \mathrm{m/s}$ and a bulk temperature of $315°\mathrm{C}$ (used for fluid parameters). [6] From the heat transfer coefficient equation derived in the Methodology section coupled with the Moody diagram, the change in the heat transfer coefficient due to the film's roughness is obtained.

Table 12: Impact on heat transfer coefficient with various film friction factors.

Film Roughness (μin)	Darcy Friction Factor (f)	Nusselt Number	Heat Transfer Coefficient $\left(\frac{\mathrm{W}}{\mathrm{cm^2K}}\right)$
5 (0.127μm)	0.014	528.26	2.97
10 (0.254μm)	0.015	566.66	3.18
15 (0.381μm)	0.016	605.13	3.40

The film's roughness shows a significant (about 10 %) change in the heat transfer coefficient between the film and the coolant. Although, the calculated heat transfer coefficient values all remain in the range of the typical Zr-coolant under normal operations, where under normal flow parameters Zr-clad has a friction factor of around 0.014. [5]

To further investigate the effect the roughness produces on the system, the pressure drop across the flow channel is evaluated. Using the same film roughness value and the perturbations (i.e. 5 and 15μin), the new pressure drop is acquired using the ΔP equation in the Methodology section. The results from this study are illustrated in Table 13.

Table 13: Pressure drop induced by film roughness along the flow channel.

Film Roughness (μin)	**Friction Factor** (f)	**Pressure Drop** (psi)
5 (0.127μm)	0.014	1.67
10 (0.254μm)	0.015	1.79
15 (0.381μm)	0.016	1.91

The small roughness values introduce a minor pressure drop along channel, all of which are below 2.0 psi. For comparison, Duderstadt gives typical pressure drop for a PWR due to friction as 0.40 bar (5.8 psi) in the core (not the full loop). This value is over double the pressure loss due to film friction. [5] The pressure drop due to channel friction is used to calculate the pumping power required to pump the coolant through the primary loop $\left(P_{\text{pump}} = \Delta P_{\text{total}} A_{\text{cs}} \bar{v}_z\right)$. If the frictional pressure drop along the channel remains smaller than the Zr-clad frictional loss, the required pumping power will decrease which can be advantageous due to the decrease in power consumption for the primary coolant pumps.

3.5: Parameter Uncertainty Analysis

To reiterate, the implementation of the ABH method for an estimate of the thermal utilization and the centerline temperature of the fuel pin are reassessed using uncertainty probability for

certain parameters. For each of the respective equations, the variables which uncertainty occurs are as follows with the corresponding percent perturbation used:

ABH Method: P_{FO} (10%) and $\Sigma_{abs}^{\mathrm{M}}$ (20%)

Centerline Temperature: h_{s} (15%) and k_{film} (20%)

To illustrate the impact the film impacts on the multiplication factor coupled with parameter uncertainties, the k_{eff} is obtained by using normal values for the other parameters in the four-factor formula (e.g. fast fission factor, reproduction factor, and resonance escape probability). [5] The standard deviations for the ABH and the centerline temperature for each film are shown in Table 14.

Table 14: Uncertainty obtained for ABH method and centerline temperature.

	Film Thickness (microns)	$\boldsymbol{\sigma_{k_{eff}}}$	$\boldsymbol{\sigma_{Temp}}$ (℃)
Reference	-	0.0113 (0.74%)	8.913 (0.49%)
ZrO_2	5	0.0108 (0.71%)	8.935 (0.48%)
TiAlN	5	0.0102 (0.67%)	8.923 (0.48%)
Ti_2AlC	5	0.0113 (0.74%)	8.921 (0.48%)
Ti_3AlC_2	5	0.0110 (0.72%)	8.920 (0.48%)
ZrO_2	10	0.0109 (0.72%)	8.924 (0.48%)
TiAlN	10	0.0110 (0.73%)	8.925 (0.48%)
Ti_2AlC	10	0.0111 (0.73%)	8.930 (0.49%)
Ti_3AlC_2	10	0.0113 (0.75%)	8.939 (0.49%)

These uncertainty (standard deviation) values are applied to the previously calculated values to illustrate the range of uncertainty within the calculation, as seen in Table 15. The multiplication factor used was obtained from the MCNP *KCODE* calculation, where, as all other parameters are not greatly impacted by the additional film region, will yield the uncertainty.

Table 15: Multiplication factor and centerline temperature with uncertainty.

	Film Thickness (microns)	$\mathbf{k}_{eff}$	$\mathbf{T_{CL}}$ (°C)
Reference	-	1.5204 ± 0.0113	1834.80 ± 8.913
ZrO_2	5	1.4896 ± 0.0108	1840.89 ± 8.935
TiAlN	5	1.4876 ± 0.0102	1837.22 ± 8.923
Ti_2AlC	5	1.4887 ± 0.0113	1835.18 ± 8.921
Ti_3AlC_2	5	1.4894 ± 0.0110	1835.07 ± 8.920
ZrO_2	10	1.4893 ± 0.0109	1847.01 ± 8.924
TiAlN	10	1.4874 ± 0.0110	1839.66 ± 8.925
Ti_2AlC	10	1.4865 ± 0.0111	1835.66 ± 8.930
Ti_3AlC_2	10	1.4871 ± 0.0113	1835.38 ± 8.939

The largest uncertainty in the multiplication factor (0.0113) is less than one percent of the calculated k_{eff} value. This is also true for the centerline temperature, where the maximum uncertainty $(8.939°C)$ is well below one percent of the centerline temperature. For the parameters selected for the uncertainty analysis coupled with the relative percent perturbations applied to each variable, the uncertainty remains minimal in both calculations.

3.6: Temperature Change during Flow Transient

To understand the impact each film introduces during the transient, each simulation will be evaluated against a reference, no-film fuel pin. The analysis is carried out using MATLAB. First, the flow velocity is varied slower than the power density, causing a momentary mismatch in fluid temperature. That is, using the previous equations from the Methodology section which expressed the time-dependent forms of the linear power density and coolant flow velocity, we

can define the equations in terms of their respective time constants (i.e. 25 seconds for the linear power density, 60 seconds for the flow velocity).

$$q'(t) = \frac{1}{2}q'(0)[\exp(-\lambda_1 t) + 1] = \frac{1}{2}q'(0)\left[\exp\left(\frac{\ln 0.5}{25}t\right) + 1\right] \quad \text{(Eq.53)}$$

$$v(t) = \frac{1}{2}v(0)[\exp(-\lambda_2 t) + 1] = \frac{1}{2}v(0)\left[\exp\left(\frac{\ln 0.5}{60}t\right) + 1\right] \quad \text{(Eq.54)}$$

As the two parameters approach a steady-state value, the change in moderator temperature in the channel rises to the original value (i.e. 20°C in our case). A linear power density value of 160 W/cm and a flow velocity of 4.0 m/s are used for initial values, respectively. Figure 10 illustrates a normal fuel pin simulation.

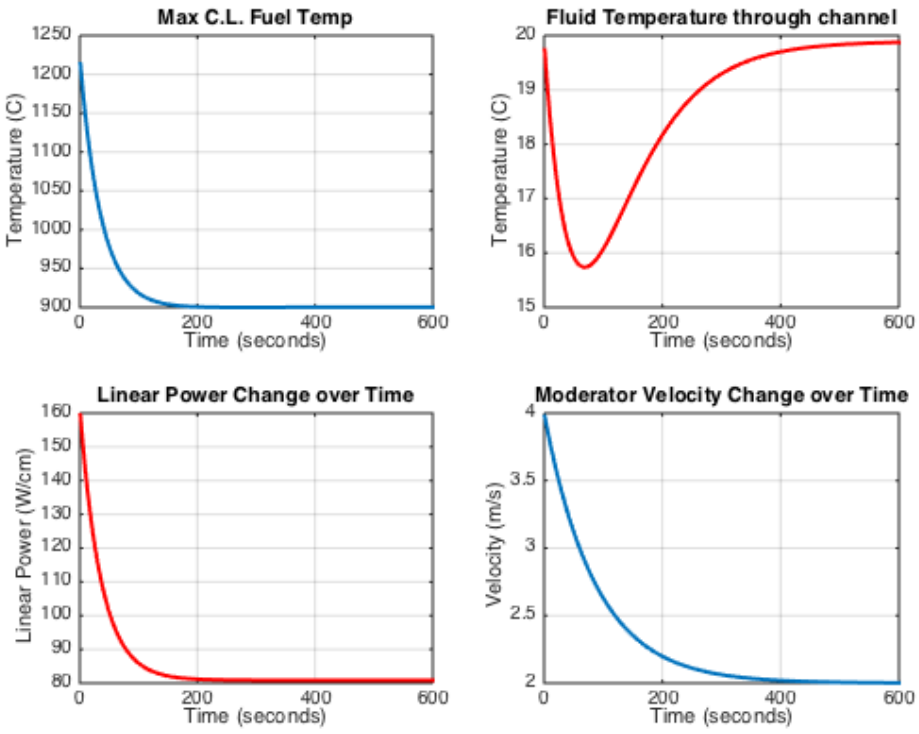


Figure 10: No-film region simulation illustrating the two varying parameters and the impact on the moderator temperature change along the channel.

From the figure, the top right plot illustrates the difference between the inlet and outlet temperature of the coolant. The transient introduces the momentary mismatch between the flow and power density, decreasing the temperature difference across the channel until both the flow and power approach a steady-state value. This simulation illustrates how the films impact the coolant's temperature difference along the channel. Additionally, the heat transfer coefficient will be decreased to adequately show the how the film's roughness can change a transient (i.e. h changed from $3.4\,\frac{\mathrm{W}}{\mathrm{cm^2K}}$ to $3.0\,\frac{\mathrm{W}}{\mathrm{cm^2K}}$ only on the film simulations).

Using the same time values to vary the flow velocity and power density, we can obtain a model for each of the films. Figures 11 through 14 illustrate each film's simulation output using a 10μm film thickness.

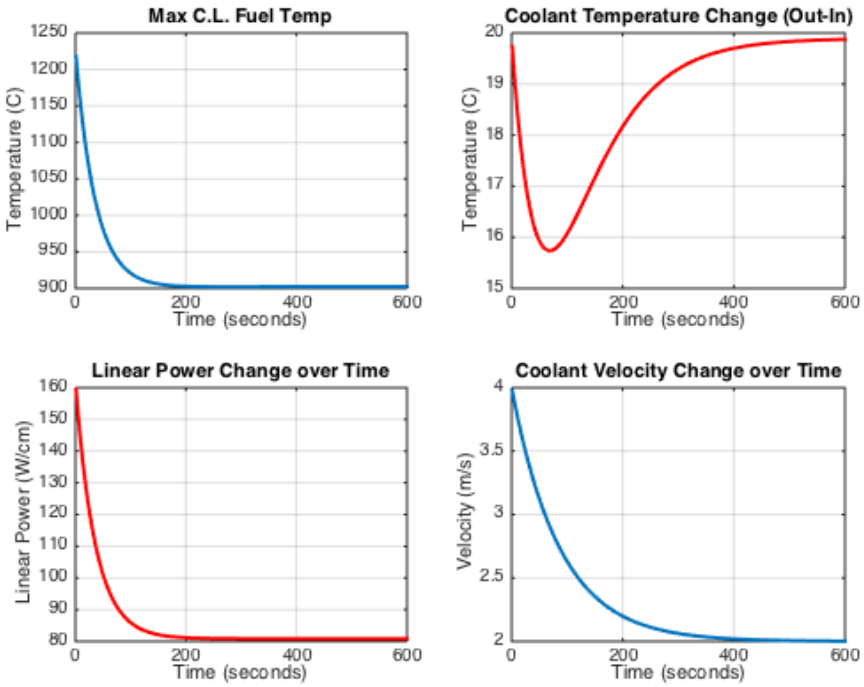


Figure 11: Power transient followed by slower velocity change using 10μm ZrO2 film.

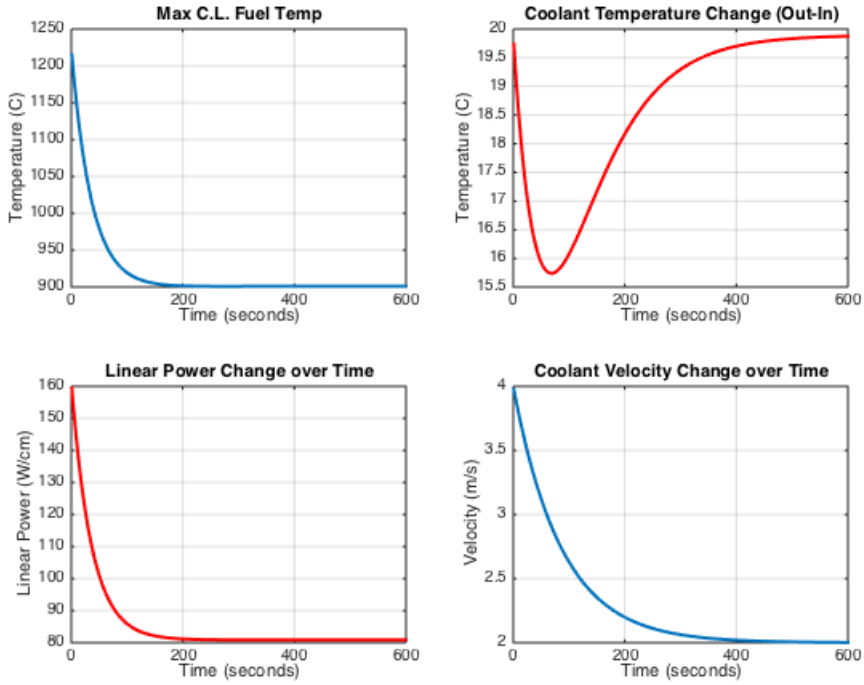


Figure 12: Power transient followed by slower velocity change using 10μm TiAlN film.

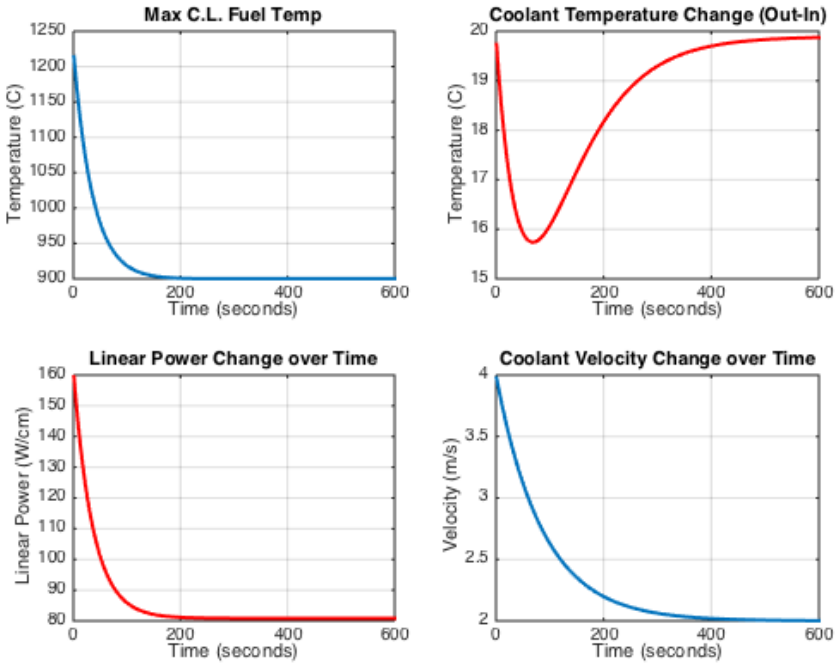


Figure 13: Power transient followed by slower velocity change using 10μm Ti_2AlC film.

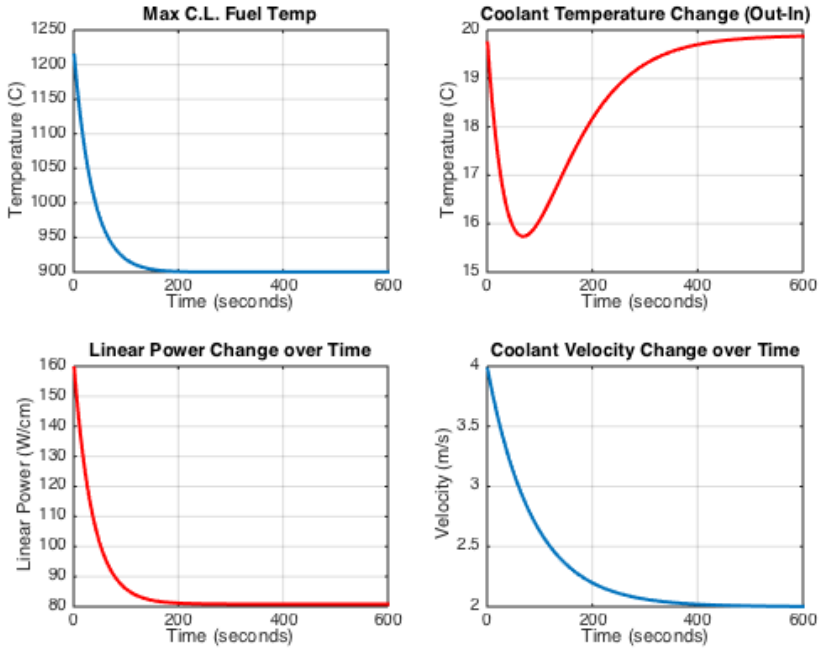


Figure 14: Power transient followed by slower velocity change using 10μm Ti_3AlC_2 film.

As a second simulation, the time constants are switched so that the flow velocity decreases sharper than the power density resulting in a momentary increase in moderator temperature across the channel (i.e. longer time change for the linear power density). Figure 15 shows the reference simulation.

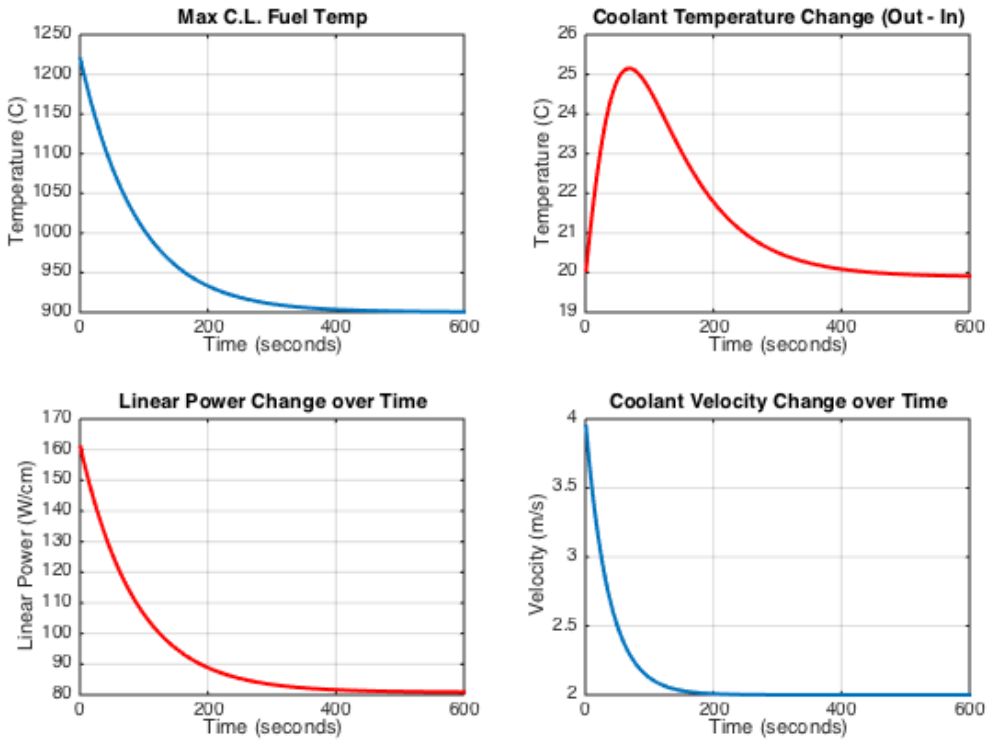


Figure 15: Reference run for flow velocity variation followed by power density.

Due to the slower power change, the outlet temperature of the coolant increases momentarily until the power and the flow both approach a steady-state value, as seen in the top right of Figure 15. That plot should be used to compare each film's impact on the peak temperature and time elapsed to become steady (i.e. validate the film has little effect on the transient). Figures 16 through 19 show each film's transient for this simulation.

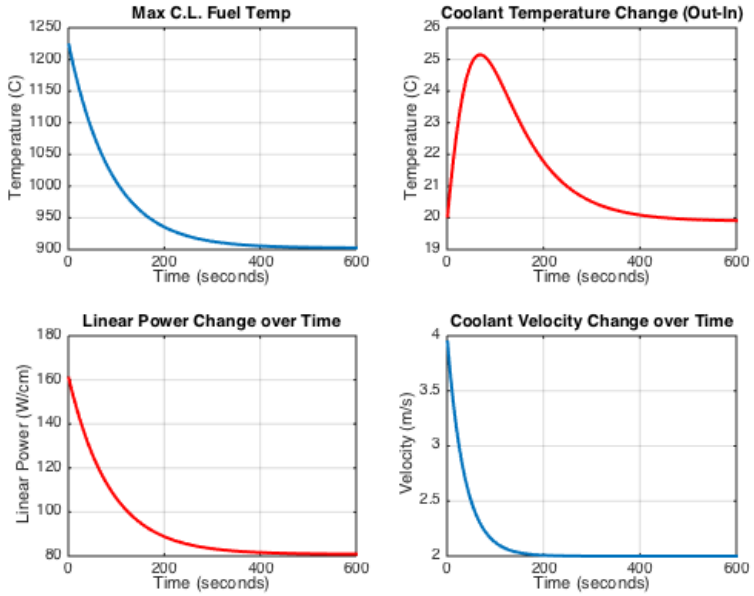


Figure 16: Flow velocity transient followed by slower power density change using 10μm ZrO_2 film and lower heat transfer coefficient.

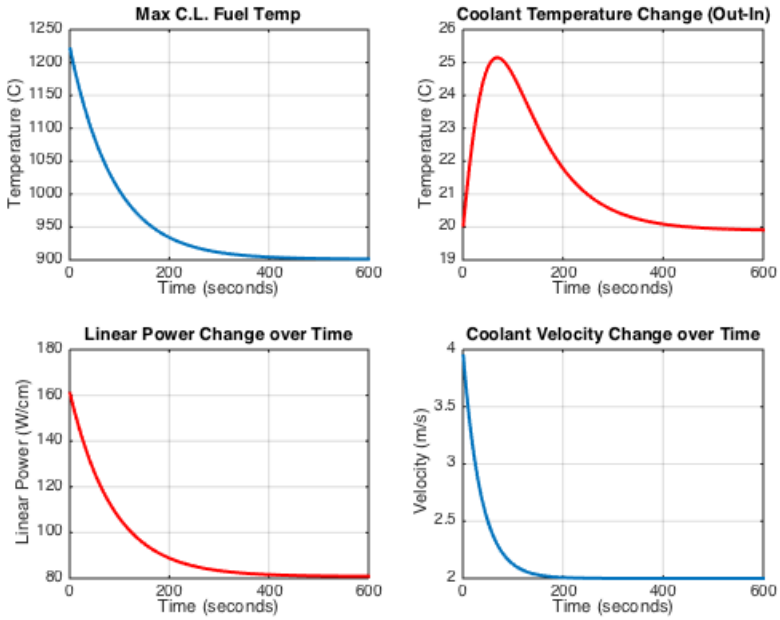


Figure 17: Flow velocity transient followed by slower power density change using 10μm TiAlN film and lower heat transfer coefficient.

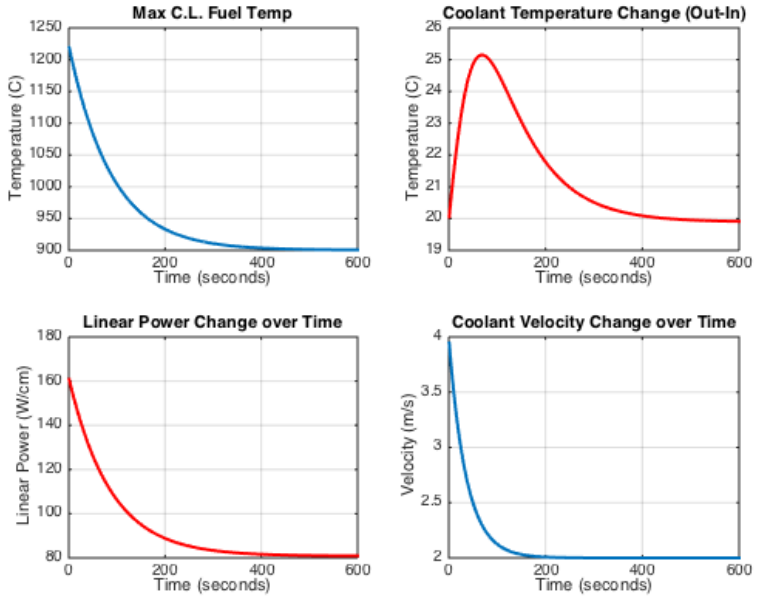


Figure 18: Flow velocity transient followed by slower power density change using 10μm Ti_2AlC film and lower heat transfer coefficient.

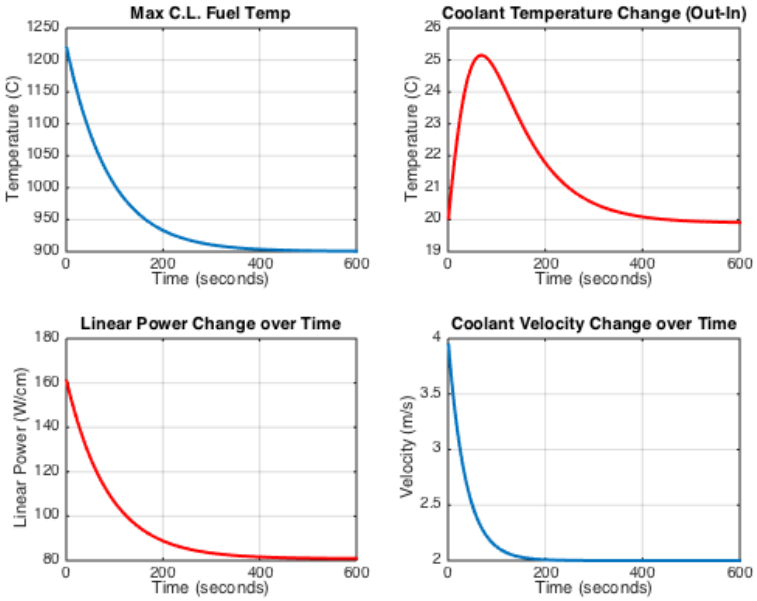


Figure 19: Flow velocity transient followed by slower power density change using 10μm Ti_3AlC_2 film and lower heat transfer coefficient.

In all film simulations, the change in moderator temperature along the channel approaches a steady state nearly identical to that of the normal fuel rod. Even using the higher thermal conductivity films (e.g. Ti_2AlC, Ti_3AlC_2) and the decrease in the heat transfer coefficient show little difference due to the small film thickness.

4: Conclusion

The assessments within this report evaluate four ceramic coatings to determine their impact on fuel performance during operation. With film thicknesses of 5 and 10 microns, the reactivity change is less than 0.5% from the reference and the corresponding increase of fuel cycle length is less than 3 days and burnup values around 48.5 MWd/kg for all cases. The maximum temperature of the fuel assessed with the film region present is well below the melting point of the fuel (maximum of $1847°C$) yielding 0.67% variation from the reference, even with high power density values of $460\ W/cm$. The roughness introduced by the film to the coolant flow channel results in small changes in heat transfer (about 10 %) and pressure change along the channel, both of which are within the Zr-alloy cladding values. During a flow and power transient, the coolant's temperature changes along the channel are about the same for all films and thicknesses relative to a reference case with no-film. The results show that thin (5 to 10 microns) ceramic films applied to the moderator/coolant side of the Zr-clad in a LWR produce small (generally less than 2%) variations in reactor performance parameters relative to those for reference conditions.

5: Future Work

In this study, material parameters were not temperature dependent; thus, further analysis is required for temperature-dependent scenarios (e.g. maximum temperature calculations). As more refined values of the film's properties become available, the calculations implemented here should be repeated. Transient analyses are also important to evaluate the film's effectiveness during normal and accident conditions (e.g. power ramps, LOCA, high temperature scenarios, etc.). Currently, the transient reactor test facility (TREAT) at Idaho National Laboratory (INL) is used to test new fuel concepts under reactor transient conditions. [15] This analysis is essential to verify the film's effectiveness during various scenarios.

Works Cited

1. *Nuclear Energy Research and Development Roadmap* - Report to Congress. United States Department of Energy. Office of Nuclear Energy. April 2010.

2. Bragg-Sitton, Shannon. "Development of advanced accident tolerant fuels for commercial LWR." Nuclear News. Pages 83-91. March 2014.

3. Bragg-Sitton, Shannon. *Advanced LWR Nuclear Fuel Cladding System Development: Technical Program Plan*. DOE Office of Nuclear Energy. December 2012. Report No. INL/MIS-12-25696.

4. *Ceramic Coatings for Clad (The C3 Project): Advanced Accident-Tolerant Ceramic Coatings for Zr-Alloy Cladding*. CFP Proposal IRP 12-4722. DOE. NEUP-IRP.

5. Duderstadt, James J. and Louis Hamilton. *Nuclear Reactor Analysis*. 1976. John Wiley & Sons, Inc.

6. Todeas, Neil E. and Kasimi, Mujid S. *Nuclear Systems: Thermal Hydraulic Fundamentals*. Volume 1. 2nd Ed. CRC Press. 2012.

7. *MCNP — A General Monte Carlo N-Particle Transport Code*, Version 5. Los Alamos National Laboratory. LA-UR-03-1987 / LA-CP-03-0245. Volume I&II. 2003.

8. Driscoll, M.J. Thomas Joseph Downar, and E. E. Pilat. *The Linear Reactivity Model for Nuclear Fuel Management*. American Nuclear Society. January 1, 1990.

9. Schmidt, Henderson, and Wolgemuth. *Introduction to Thermal Sciences*. John Wiley & Sons. 2nd ed. 1993.

10. *@Risk Analysis Software using Monte Carlo Simulations for Excel*. Palisade Corporation. Ithaca, NY. 2014. <https://www.palisade.com/risk/>.

11. Rasmussen, Inge. *Optical Monitoring and X-ray Absorption Spectroscopy for Studies of Wear on Thin Films*. December 2010. <http://www.nbi.ku.dk/english/research/phd_theses/phd_theses_2011/inge_l_rasmussen/inge_l_rasmussen.pdf>.

12. *Zirconia: Ceramic Properties Tables*. Ferro Ceramic Grinding, Inc. Willmington, MA. <http://www.ferroceramic.com/zirconia.htm>.

13. *About ZrO2*. K-Style Advanced Ceramics. P.R. China. 2006. <http://www.zro2.com/Top-About-ZrO2.htm>.

14. "Cross Section Metallography of TiAlN Coated ZIRLO." Ceramic Coating of Cladding Meeting. Pennsylvania State University. 12 July 2013. Lecture.

15. Ehresman, *Teri.* "Transient Reactor Test Facility." US DOE. Idaho National Laboratory. Web. Jan. 2015. <http://www.inl.gov/research/transient-reactor-test-facility>.

Appendix

Various calculations and techniques were also undertaken during the study, some of which was insignificant or deemed unnecessary after finishing the analysis. Following this is the evaluation of film depletion and new high absorbing film compounds.

Film Depletion Approximation

Depletion of the ceramic films during operation is important in understanding how the film will respond over the lifetime of the fuel. In order to estimate the depletion of an isotope, there are two standard approximations, constant power and constant flux. These approximations for isotropic depletion are quite different, as illustrated in Figure 20 below. [5]

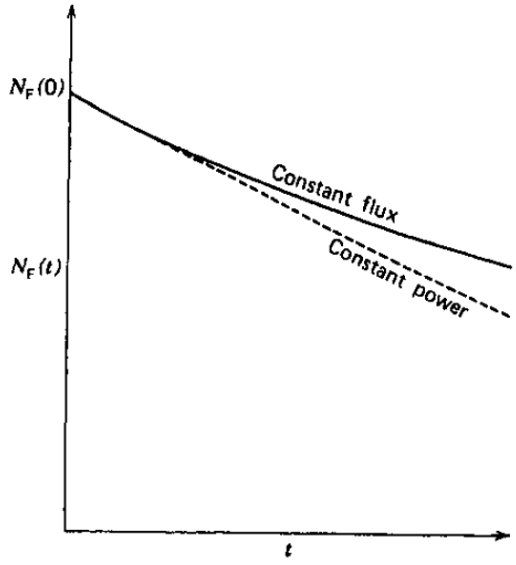


Figure 20: Depletion of a single isotope comparison using constant flux and constant power approximations.

Constant Flux Approximation

Assuming that over the lifetime of the fuel the flux is treated as constant, the number density of an isotope can be approximated. That is, the burnup or depletion of an isotope can be expressed by the simple rate equation: [5]

$$\frac{dN}{dt} = -N(r,t)\,\sigma_{\text{abs}}\,\phi(r,t) \qquad \text{(Eq.55)}$$

Thus by assuming a constant flux over the lifetime of the fuel:

$$\phi(r,t) = \phi_0 \qquad \text{(Eq.56)}$$

$$N(t) = N(0)e^{-(\sigma_{\text{abs}}\,\phi_0\,t)} \qquad \text{(Eq.57)}$$

Constant Power Approximation

By assuming a constant reactor power, the depletion of the number density of an isotope can be obtained. This implies:

$$\frac{dN}{dt} = -\sigma_{abs}\,N\,\phi = \frac{P_0}{w_a} \qquad \text{(Eq.58)}$$

Where, w_a is the energy released per neutron absorption ($w_a = \left(\frac{\sigma_f}{\sigma_a}\right) w_f$).

By integrating this equation, one finds:

$$N(r,t) = N(r,0) - \frac{P_0(r)}{w_a}\,t \qquad \text{(Eq.59)}$$

This equation differs greatly from that of the constant flux approximation. However, over short time intervals, the solutions of both approximations are similar, since the previous constant power equation becomes: [5]

$$N(r,t) \cong N(r,0)[1 - \sigma_{abs}\phi_0 t] \quad \text{(Eq.60)}$$

Using a constant flux value of $10^{13}\,\frac{\mathrm{n}}{\mathrm{cm-s}}$, the isotropic depletion of the three ceramic films were calculated via MATLAB using both approximations. Table 16 lists the isotope depletion using the constant power approximation and Table 17 lists the depletion using the constant power approximation. Both calculations use a fuel cycle length of 1000 days.

Table 16: Depletion of each film isotope using constant power approximation equation.

Film	Isotope	Flux Approximation (n /cm-s)	Isotope Depletion (%)
ZrO_2	Zr	10^{13}	0.08%
	O	10^{13}	8.65E-5%
TiAlN	Ti	10^{13}	2.51%
	Al	10^{13}	0.10%
	N	10^{13}	0.81%
Ti_3AlC_2	Ti	10^{13}	2.51%
	Al	10^{13}	0.10%
	C	10^{13}	0.002%

Table 17: Isotropic Depletion using constant flux approximation equation.

Film	Isotope	Flux Approximation (n /cm-s)	Isotope Depletion (%)
ZrO_2	Zr	10^{13}	0.07%
	O	10^{13}	$8.63E$-5%
TiAlN	Ti	10^{13}	2.48%
	Al	10^{13}	0.10%
	N	10^{13}	0.80%
Ti_3AlC_2	Ti	10^{13}	2.48%
	Al	10^{13}	0.10%
	C	10^{13}	0.001%

High Absorption Films

Preliminary evaluation of new film compounds was also conducted. A heavy absorber material is proposed to be added to the film, which could be beneficial to the system. Such isotopes with high absorption cross sections that are within a nuclear reactor are boron, gadolinium, indium, and xenon. To assess the impact an isotope with a high absorption cross-section yields on the system, two films are utilized: B_4C and BN.

MCNP and the ABH method are both used to evaluate the change in the multiplication factor (k). Both films are assessed at 10 micron and 100 micron thicknesses. In order to lessen the initial affect the high absorption cross section of the ^{10}B isotope ($\sigma_a \cong 3850\ b$), a ratio of ^{10}B to ^{11}B is used (natural boron is roughly 80% ^{11}B and 20% ^{10}B). Three ratios are used:

1. 20% ^{10}B, 80% ^{11}B
2. 1% ^{10}B, 99% ^{11}B
3. 0.1% ^{10}B, 99.9% ^{11}B

The cross-section library used for this analysis is for (n, γ) reactions. Tables 18 and 19 list the change k_{eff} using MCNP and the ABH method for 10 micron and 100 micron thicknesses.

Table 18: Multiplication factor with varying boron concentration ratios at 10-micron film.

Film	Thickness	B-10 / B-11 Concentration	k_{eff} (MCNP)	Difference (MCNP)	Difference (ABH)
Reference	-	-	1.520	-	-
B_4C	10	20% / 80%	1.016	33.14%	25.84%
B_4C	10	1% / 99%	1.477	2.84%	1.64%
B_4C	10	0.1% / 99.9%	1.516	0.29%	0.10%
BN	10	20% / 80%	1.127	25.84%	48.30%
BN	10	1% / 99%	1.488	2.10%	4.60%
BN	10	0.1% / 99.9%	1.515	0.35%	0.62%

Table 19: Multiplication factor for different boron concentration ratios at 100-micron film.

Film	Thickness	B-10 / B-11 Concentration	k_{eff} (MCNP)	Difference (%)	Difference (ABH)
Reference	-	-	1.520	-	-
B_4C	100	20% / 80%	0.389	74.38%	77.30%
B_4C	100	1% / 99%	1.192	21.56%	14.02%
B_4C	100	0.1% / 99.9%	1.489	2.05%	0.94%
BN	100	20% / 80%	0.464	69.49%	88.38%
BN	100	1% / 99%	1.265	16.79%	28.11%
BN	100	0.1% / 99.9%	1.469	3.38%	4.69%

From Table 18 and 19 it should be noted the impact ^{10}B produces to the multiplication factor. The films would most likely be destroyed, thus changing the atomic compound of the film. The impact on fuel cycle is not shown here and is more difficult to understand than the other four films considering the boron deplete fairly rapids and burn out at the beginning of the fuel life cycle. This quick depletion could be useful when attempting to compensate for excess reactivity during early stages of core life.

PWR Data

The information on parameters for the PWR analysis used the values from in *Nuclear Reactor Analysis* by Duderstadt and Hamilton. [5]

Table 20: Reactor Information from Duderstadt text Appendix H. [5]

General Data	**PWR (Westinghouse)**
Thermal Output (MWth)	3411
Electrical Output (MWe)	1150
Efficiency (%)	33.7
Fuel Type	UO_2
Coolant	H_2O
Structural Material	Zircaloy
Moderator	H_2O
Core Data	
Active Height (cm)	366
Equivalent Active Diameter (cm)	337
Height / Diameter	1.09
Active Core Volume (L)	32,800
Average Core Power Density (kW/L)	104
Fuel Weight (kg)	90,200
Specific Power (kW/kgU)	37.8
Burnup (MWd/MTU)	33,000
C.R.	0.5
Fuel Type Assembly	Square Bundles
Number of Assemblies	193
Fuel-element array	17 x 17
Assembly Dimension (cm)	21.4 x 21.4
Assembly Pitch (cm)	21.5
Number of Fuel Elements / Assembly	264
Total Number of Fuel Locations	50,952
Fuel Element Date Type	Clad rod
Fuel-element Pitch (cm)	1.25
Fuel Element O.D. (cm)	0.94
Pitch / Diameter	1.32
Clad Thickness (cm)	0.0572
Fuel-pellet diameter (cm)	0.819
Pellet-Clad Gap (cm)	0.0082
Fuel Enrichment	2.1/2.6/3.1
Thermal Hydraulic Data	
System Pressure (bar)	155
Coolant Flow (10^6 kg/hr)	62
Average Linear Power Density (W/cm)	178
Maximum Linear Power Density (W/cm)	426
Average Heat Flux (W/cm^2)	68.5
Maximum Heat Flux (W/cm^2)	183
Minimum DNBR	1.3
Inlet Temperature (C)	300
Outlet Temperature (C)	332
Maximum Fuel Temperature	1788

Code Implementation

Example MCNP multiplication factor calculation (KCODE) for Ti_2AlC film at 10micron thickness. Single fuel pin, infinite in length, with 5 regions present: fuel, gap, clad, film, and moderator. The enrichment used is 5% U-235 with 95% U-238. The k_{eff} calculation implemented 1000 histories per cycle, an initial guess of 1.0, with 1000 cycles total, while skipping the first 50. It should be noted that the format shown here may be different due to formatting issues within the report, but the syntax is correct.

```
MCNP Analysis of Ti2AlC Ceramic Film
C ---------------
C Cell
C ---------------
1 1 -10.96 -1 imp:n=1       $ fuel
2 0    1 -2 imp:n=1         $ gap
3 2 -6.49 2 -3 imp:n=1      $ clad
4 3 -4.1 3 -4 imp:n=1       $ Ti2AlC film
5 4 -0.9982 4 -5 imp:n=1    $ moderator
0 0         5 imp:n=0       $ end void

C ---------------
C Surface
C ---------------
1 CY 0.4095
2 CY 0.4177
3 CY 0.4749
4 CY 0.4759          $ 10 micron thickness
+5 CY 0.70524 $+ indicates white boundary

C ---------------
C Data
C ---------------
mode n
M1   8016  2.0       $ UO2 Fuel
       92235  0.05
       92238  0.95
M2 40090 1.0         $ Zr Clad
M3 22048 2.0 13027 1.0 6012 1.0 $ Ti2AlC Film
M4 1001 2.0 8016 1.0 $ H2O Mod
kcode 1000 1.0 50 1000 $ Keff: 1000histories/cycle, 1 K_guess, first 50
cycles of 1000 skipped
ksrc 0 0 0           $ Keff Source location (x,y,z)
print
```

The ABH method used to expand the thermal utilization factor within the four-factor formula is shown here. The code is written within MATLAB software, with each film having its own code (ran into syntax errors when compiled all four films into one). Here is an example for Ti_2AlC film at a 5 micron thickness. Again, readers are warned that due to formatting in report, certain line-movement, syntax, etc., the code may present certain errors due to this formatting.

```
%% Inputs/Assumptions, Westinghouse PWR Parameters / Appendix H Duderstadt
    Dpin = 0.819;       %Fuel Pin Diameter (cm)
    Pitch = 1.25;       % (cm)
    a = Dpin/2;         %Fuel radius (cm)
    b = Pitch/(pi^0.5); %Moderator-Cell Radius (cm)
    ACell = Pitch^2;    %Area of cell (cm^2)
    rFuel = Dpin/2;     % cm (radius of the fuel element)
    tGap = 0.0082;      % cm (thickness of the air gap)
    tClad = 0.0572;     % cm (thickness of the cladding)
% Volume Fractions
    Vf = (rFuel^2*pi)/(Pitch^2); %Fuel Volume (assume 1cm length) (cm^3)
    Vgap = ((pi*(rFuel+tGap)^2)-Vf)/(Pitch^2);
    Vclad = (pi*((rFuel+tGap+tClad)^2)-(Vf+Vgap))/(Pitch^2);
    tFilm = 0.0005; %Film Thickness (cm)
    VFilm = ((pi*(rFuel+tGap+tClad+tFilm)^2)-
(pi*(rFuel+tGap+tClad)^2))/(Pitch^2);
    Vm = (ACell-(pi*(tGap+tClad+rFuel+tFilm)^2))/(Pitch^2);
    Vm1 = (ACell - (pi*(tGap+tClad+rFuel)^2))/ACell; % Mod Vol w/out film
    coatings = {'Ti2AlC'};
% Film Data %
    Nav = 6.02*(10^23); %Avogadro's Number (Atom/Mole)
    dTi2AlC = 4.0; %Density Ti2AlC Film (g/cc)
    WTi2AlC = 134.726; %Atomic Weight Ti2AlC (g/mole)
    NTi2AlC = (Nav*dTi2AlC)/WTi2AlC; %No. Density Ti2AlC (1/cc)
    SigmaTi2AlC = 11.8*10^-24; %Abs. MicroCS (b to cm^-2)
    %Macroscropic Cross-section for Ceramic Films:
    SigmaFilm = SigmaTi2AlC*NTi2AlC;
% Macroscopic Cross-sections from Appendix H in Duderstadt %
    SigmaMa = 0.022;    %Abs. MacroCS Moderator (cm^-1)
    SigmaFa = 0.169;    %Abs. MacroCS Fuel (cm^-1)
    SigmaFs = 0.372;    %Scatter MacroCS Fuel (cm^-1)
    SigmaFt = SigmaFa+SigmaFs; %Total MacroCS Fuel (cm^-1)
    SigmaMt = 3.45;     %Total MacroCS H2O (cm^-1)
    SigmaMs = 3.45;     %Scatter MacroCS H2O (cm^-1)
    SigmaMa1 = (Vm/(Vm+VFilm)*SigmaMa)+(SigmaFilm*VFilm/(Vm+VFilm)); %Volume
Avg. MacroCS
    u_o = 1-0.676;      %App.A for H2O
    lMtr = (SigmaMt-(u_o*SigmaMs))^-1; %Eq.4-150 Duderstadt, m.f.p. Moderator
    Diff_length = 0.7104*lMtr;
    Lm = (Diff_length/SigmaMa)^0.5; %Used in Lattice Function
    S_f = pi*Dpin; %Surface Area of Fuel region (pi*D)*1cm
% Fig.10-11 Duderstadt for ABH method %
    abh = a*SigmaFt;
    alpha = -0.0064*abh^2 + 0.0679*abh + 0.0022; %Best fit f(x)-
    beta = -0.0038*abh^2 + 0.0162*abh + 0.0122;  %-for Fig.10-11
% Fig.10-13 Duderstaft for extrapolation dist. (d)
    RMtr = Pitch/pi^0.5/lMtr;
    d = 0.7104*lMtr;
% Bessel Functions for Lattice Fuction %
```

```
    I0a = besseli(0,a/Lm);
    K0a = besselk(0,a/Lm);
    K1a = besselk(1,a/Lm);
    I1a = besseli(1,a/Lm);
    I1b = besseli(1,b/Lm);
    K1b = besselk(1,b/Lm);
% Bessel Functions for Lattice Function with Film Cross-Section added %
    lMtrf = ((SigmaMa1+SigmaMt)-(u_o*SigmaMs))^-1; %Eq.4-150 Duderstadt,
m.f.p. Moderator
        d_film = 0.7104*lMtrf;
        Lmf = (d_film/SigmaMa1)^0.5;
            I0af = besseli(0,a/Lmf);
            K0af = besselk(0,a/Lmf);
            K1af = besselk(1,a/Lmf);
            I1af = besseli(1,a/Lmf);
            I1bf = besseli(1,b/Lmf);
            K1bf = besselk(1,b/Lmf);
   %% Calculations
    Pfo = S_f/(4*Vf*SigmaFa); %First-Flight Escape Prob. Approx. Eq.10-49
Duderstadt
    %Reference Run
        Lattice = ((b^2-a^2)/(2*a*Lm))*((I0a*K1b+K0a*I1b)/(I1b*K1a-K1b*I1a));
%Lattice Function
        fREF = (((SigmaMa*Vm1)/(SigmaFa*Vf))*(1+(SigmaFa/SigmaFt)*((1-
Pfo)/Pfo-a*SigmaFt)*(1+alpha*(SigmaFs/SigmaFt)...
            + beta*(SigmaFs/SigmaFt)^2))+((a*d/(2*Lm^2))-
a*SigmaMa)*(Vm1/Vf)+Lattice)^-1; %Reference Thermal Utilization
        fprintf(1,'The thermal utilization for the reference run without the
film region is %0.4f.\n',fREF);
    %Film Runs
        LatticeFilm =((b^2-a^2)/(2*a*Lmf))*((I0af*K1bf+K0af*I1bf)/(I1bf*K1af-
K1bf*I1af));
        fFILM = (((SigmaMa1*Vm)/(SigmaFa*Vf))*(1+(SigmaFa/SigmaFt)*((1-
Pfo)/Pfo-a*SigmaFt)*(1+alpha*(SigmaFs/SigmaFt)...
                + beta*(SigmaFs/SigmaFt)^2))+((a*d/(2*Lmf^2))-
a*SigmaMa1)*(Vm/Vf)+Lattice)^-1;
        Difference = abs((fFILM-fREF)/fREF*100);
        s = coatings{1};
    fprintf(1,'The thermal utilization for the %5s film run is %0.4f.\nThe
percent change from the reference is %2.3f percent for a %0.0f-micron film
thickness.\n',...
        s,fFILM,Difference,tFilm*1E4);
```

Presented below is the one-dimensional thermal analysis using the circuit analogy. The code is written and implemented using MATLAB. All four films and thicknesses (i.e. 5 and 10 microns) are implemented in the code. The percentages calculated are found via the reference run also within the code.

```
clear all; clc;
%% Thermal Analysis of the effects Coatings
rFuel = 0.4095;      % cm (radius of the fuel element)
tGap = 0.0082;       % cm (thickness of the air gap)
tClad = 0.0572;      % cm (thickness of the cladding)
qPrime = 460;        % W/cm (Linear Power Density, pg. 419 Nuc Sys)
kFuel = 0.025;       % W/cm K (thermal conducitivity of fuel)
Rg = rFuel + tGap/2;% cm (Average radius of air gap)
hg = 0.75;           % W/cm^2 K (heat transfer coefficient gap, pg. 419 Nuc
Sys)
kClad = 0.1070;      % W/cm K (thermal conducitity of the clad)
Rci = rFuel + tGap; % cm, (inner cladding radius)
Rco = Rci + tClad;  % cm (outer cladding radius)
h = 3.3;             % W/cm^2 K (heat transfer coefficient of water to film)
%% Reference Fuel Case
% The reference fuel pin does not have the coating
Roo = Rco;
deltaTRef = qPrime/(2*pi)*(1/(2*kFuel)+ 1/(Rg*hg) + log(Rco/Rci)/kClad +
1/Roo/h);
deltaTRefClad = qPrime/(2*pi)*(log(Rco/Rci)/kClad + 1/Roo/h);
fprintf(1,'The change in temperature across a reference fuel pin: %5.2f
K\n',deltaTRef);
fprintf(1,'The change in the inner cladding radius: %5.2f
K\n',deltaTRefClad);
%% Different Coatings
coatings = {'ZrO_2','TiAlN','Ti_2AlC','Ti_3AlC_2'};
k = [2, 5, 30, 40]/1000;   % W/cm k (thermal conducivity of film coating)
sigma = [0.01, 0.001]; % cm (thickness of coating)
deltaTFuel =  @(ko,sigmao) qPrime/(2*pi)*(1/(2*kFuel)+ 1/(Rg*hg) +
log(Rco/Rci)/kClad + 1/(2*pi*(Rco+sigmao)*ko/sigmao)+1/Roo/h);
deltaTClad =  @(ko,sigmao) qPrime/(2*pi)*(log(Rco/Rci)/kClad +
1/(2*pi*(Rco+sigmao)*ko/sigmao)+1/Roo/h);
precentChange = @(T) (T-deltaTRef)/deltaTRef*100;
for j = 1:numel(sigma)
    fprintf(1,'%3.0f um Coating \t\t   Fuel Pin\t Cladding Outer\t  Reference
\t Precent Change\n',sigma(j)*1E4);
    fprintf(1,'\t\t\tk_film  \tTemperature \tDelta T\n');
    for i=1:numel(coatings)
        dT = deltaTFuel(k(i),sigma(j));
        dTClad = deltaTClad(k(i),sigma(j));
        s = coatings{i};
        fprintf(1,'%10s (%3.0f W/cm-K) \t %5.2f \t %5.f \t\t %6.2f \t %5.4f
\n',...
            s,k(i)*1000,dT,dTClad,dT-deltaTRef,precentChange(dT));
    end
end
```

Roughness impact on the heat transfer coefficient and pressure drop along the flow channel is shown below. The code is written in MATLAB and shows three friction factors (see Moody diagram) of 0.014, 0.015, and 0.016.

```
% Evaluation of Relative Roughness Impact on heat transfer coef.
clear all; close all; clc;
%% Problem Calculations
 film_thickness = 0.01; %cm (100micron)
 fuel_diameter = 0.95; %cm
 d_hydraulic = (fuel_diameter+2*film_thickness);
 flow_velocity = 400; %cm/s
% Moderator Values (H20 at 300C, Intro. Thermal Sciences by Schmidt)
 mu = 0.0858*10^-3; %kg/m-s Viscosity
 cp = 5.78; %J/g-C Specific Heat
 k = 0.545; %W/m-C Thermal Conductivity
% Heat Transfer values and roughness
 friction = [0.014,0.015,0.016]; %See Moody Chart
 Re = (flow_velocity*d_hydraulic)/(100*100*0.1205*10^-6)
 Pr = (cp*mu*1000)/k; %Prandtl #
for i=1:length(friction)
 Nu(i) = ((friction(i)/8)*(Re-
1000)*Pr)/(1+12.7*sqrt(friction(i)/8)*(Pr^(2/3)-1)); %Nusselt #
 h(i) = (k/100*Nu(i))/d_hydraulic;
 delta_P =
1000*9.81*(friction(i)*(400/d_hydraulic)*(flow_velocity/100/(2*9.81)))/1000;
 fprintf('Heat transfer coefficient (h) for %.3f (Darcy) friction
factor:%5.2f W/cm2-K\n',friction(i),h(i));
 fprintf('\tPressure drop: %.2f kPa (%.2f
psi)\n',delta_P,delta_P*0.145037738);
end
```

Transient analysis for varying time-dependent flow velocity and power density is shown below. MATLAB is used for the analysis. In this example, the power density is varied faster (25seconds) than the flow velocity (60seconds), creating a momentary decrease in coolant temperature change along the channel. All films are implemented with the code at a thickness of 10 microns.

```
% Approx. Fuel CL Temp. with exponential change in q' & mass flow
% For each film, only the thermal conductivity will change and thickness.
% Multiple flows are given to understand the placement (up the rod) and
%   the change in the centerline temperature.
% The electrical resistor analogy is used for linear heat transfer
%   across the fuel pin.
clear all; clc; close all; format compact;
%% FILM Properties %%
 sigma = 0.001;      %Coating Thickness (cm)
 films = {'ZrO2','TiAlN','Ti2AlC','Ti3AlC2'};
 kFilm = [2,5,30,40]/1000;     %W/cm-K (thermal cond. of film)
%% Fuel/Flow Properties %%
 Tin = 295+273;      %K (Initial Temp.)
 rFuel = 0.4095;     %cm (Radius of the fuel element)
 H = 12*12*2.54;     %cm (Assuming 12ft fuel assembly length)
 A = 0.824;          %cm^2 (Cross-sectional flow area)
 v0 = 4*100;         %cm/s (H20 flow rate)
 rho = 0.001;        %kg/cc (H2O density, Table K.2 in Todreas p.975)
 m0 = rho*A*v0;      %kg/s (H2O mass flow)
 cp = 5.742E3;       %J/kg-K (Coolant Specific heat, Todreas p.975)
% Initial Power based on 5-m/s flow
 q0 = (rho*A*500*cp*(25)/H);
%
 kFuel = 0.025;      %W/cm-K (U-fuel thermal cond.)
 tGap = 0.0082;      %cm (Gap Thickness)
 Rg = rFuel + tGap/2;%cm (Average radius of air gap)
 hg = 0.75;          %W/cm^2 K (heat transfer coefficient gap, pg. 419 Nuc
Sys)
 tClad = 0.0572;     %cm (thickness of Zr-cladding)
 kClad = 0.1070;     %W/cm K (thermal conductivity of the fuel)
 Rci = rFuel + tGap; %cm (inner cladding radius)
 Rco = Rci + tClad;  %cm (outer cladding radius)
 hs = 3.4;           %W/cm^2-K (heat transfer coefficient of water to clad)
 Roo = Rco + sigma;  %cm (radius to outside film)
 visc_k = 0.13E-2;   %cm^2/s (kinematic viscosity at 300-C)
 Re=(v0*2*Roo)/visc_k; %Unitless (Reynolds No. used with Moody Chart)
%% Calculations %%
z=0; %Starting position
for k=1:length(films) %Stepping through films
 for t=1:600 %Time steps in Seconds (due to eigenvalues-lambdas in sec^-1)
  %qPrime(t) =
(dTfluid*m0*cp*(exp(log(0.25)/60*t)+1))/(exp(log(0.25)/100*t)+1); %Fixed
  qPrime(t) = (0.5*q0*(exp(log(0.5)/25*t)+1)); %Linear Power change to 0.5q0
  v(t) = 0.5*v0*(exp(log(0.5)/60*t)+1); %Flow velocity change to 0.5m0
  m(t) = rho*A*v(t); %kg/s (H2O mass flow)
   for i=1:145
    Tr1(i) = Tin-((qPrime(t)*H/m(t)/cp/pi)*(cos(pi*z/H)-1));
```

```
    T1(i) =
qPrime(t)*sin(pi*z/H)/(2*pi)*(1/(2*kFuel)+1/(Rg*hg)+log(Rco/Rci)/kClad+1/(2*p
i*(Rco+sigma)*kFilm(k)/sigma)+1/Roo/hs);
    T_CL(i) = Tr1(i) + T1(i);
    z=z+2.54;
   end
  z=0; %Resets position for next time interval
  Delta_TFluid(t)=Tr1(145)-Tr1(1); %Change in mod temp for each time step
  Max_CL_Film(t)=max(T_CL); %Assigning T_CL Max for each time step
end
%% Plots
figure(k)
 subplot(2,2,1)
 plot(Max_CL_Film,'Linewidth',2)
 title('Max C.L. Fuel Temp','FontWeight','bold')
 xlabel('Time (seconds)');
 ylabel('Temperature (C)');
 grid on
 subplot(2,2,2)
 plot(Delta_TFluid,'-r','Linewidth',2)
 title('Fluid Temperature through channel','FontWeight','bold')
 xlabel('Time (seconds)');
 ylabel('Temperature (C)');
 grid on
 subplot(2,2,3)
 plot(qPrime,'-r','Linewidth',2)
 title('Linear Power Change over Time','FontWeight','bold')
 xlabel('Time (seconds)');
 ylabel('Linear Power (W/cm)');
 grid on
 subplot(2,2,4)
 plot(v/100,'Linewidth',2)
 title('Moderator Velocity Change over Time','FontWeight','bold')
 xlabel('Time (seconds)');
 ylabel('Velocity (m/s)');
 grid on
end
```

Vita

Ian Stewart graduated from the University of Tennessee in Knoxville, TN in 2013 with a Bachelor of Science in Nuclear Engineering. Following graduation, Ian enrolled at the University of Tennessee to pursue his Doctorate in Nuclear Engineering. Upon completion of his Master's degree under Dr. L.F. Miller, Ian will join Dr. Howard Hall's group at the University of Tennessee for his Doctorate. His interests within the nuclear field have narrowed to nuclear safeguards/security and radiation transport. Ian's professional goals are to work on an international level in nuclear security and non-proliferation.